SPECTROSCOPY

(GAS)

Muhammad Aslam Baig

Quaid-i-Azam University
Islamabad, PAKISTAN

JASS' 02

October 19-28, 2002
Jordan

ABSORPTION STUDIES:

- Precise Energy Level Measurements
- Photoionization Cross Section
- Many- Body Effects / Double Excitation
- Configuration Interaction

ZEEMAN SPECTROSCOPIC STUDIES:

- Total Angular Momentum Assignments
- Wavefunction Mixing Determinations
- g - values
- Inter n,l- Mixing
- Quasi Landau Resonances

MAGNETO - OPTICAL STUDIES:

- Oscillator Strengths Measurements
- Relative f-values Measurements

PRACTICAL APPLICATIONS:

- Chemical abundances determinations:

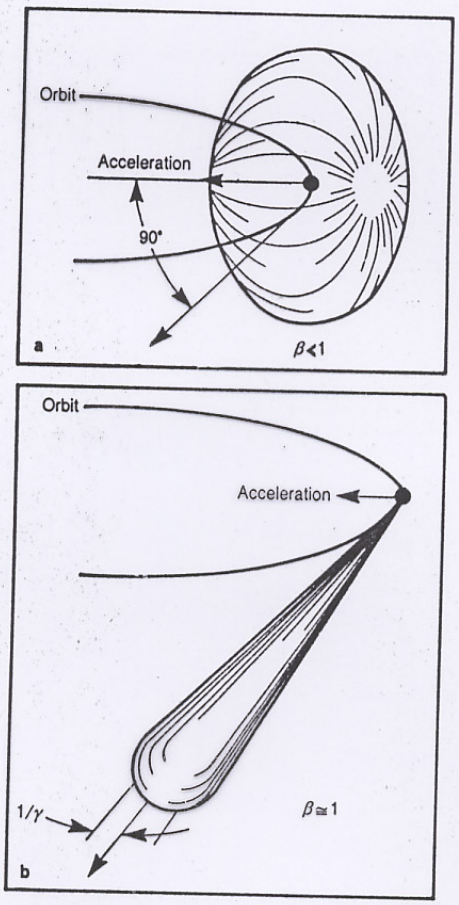

Radiation pattern of electrons in a circular orbit. The upper diagram shows the pattern for nonrelativistic electrons predicted by Joseph Larmor. The lower diagram shows the pattern for highly relativistic electrons: the radiation is concentrated in a narrow cone; the spectrum also extends to very high frequencies.

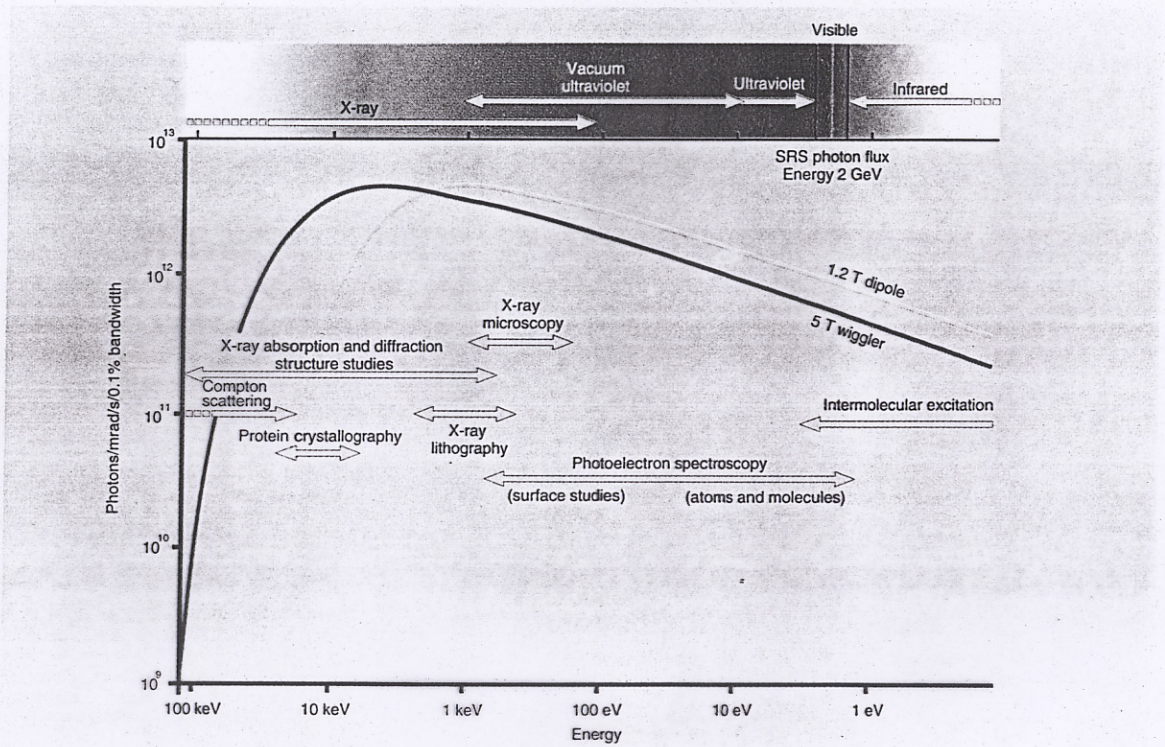
Visible
Vacuum ultraviolet
Ultraviolet
Infrared
X-ray
SRS photon flux
Energy 2 GeV
1.2 T dipole
5 T wiggler
X-ray microscopy
X-ray absorption and diffraction structure studies
Compton scattering
Protein crystallography
X-ray lithography
Intermolecular excitation
Photoelectron spectroscopy
(surface studies)
(atoms and molecules)
Photons/mrad/s/0.1% bandwidth
10^{13}
10^{12}
10^{11}
10^{10}
10^{9}
100 keV
10 keV
1 keV
100 eV
10 eV
1 eV
Energy

EXPERIMENTAL SET UP

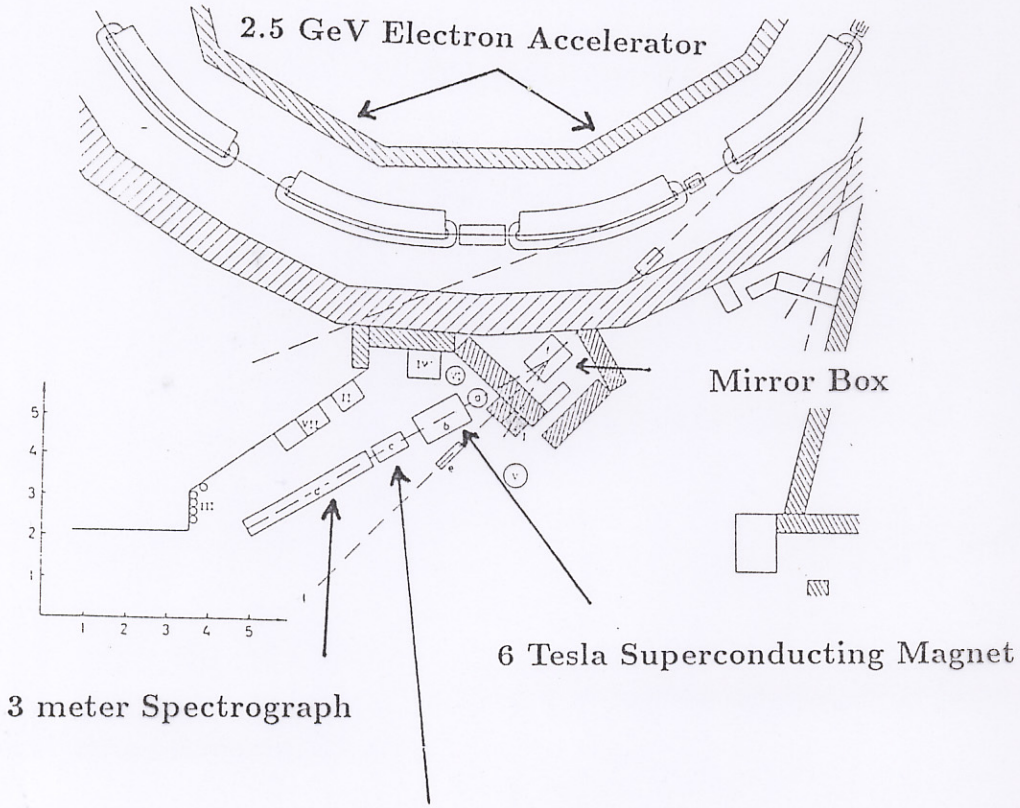

3 Meter Spectrograph

- MOUNTING: EAGLE, OFF PLANE
- GRATING: Holographic
  Al + MgF_2 overcoated
  5000 lines/mm
  50 x 50 mm
- RADIUS: 300 cm.
- SLIT: 20 – 30 μm.
- RESOLVING POWER:

$$P_E = \frac{\lambda}{\Delta\lambda} = \frac{2F(\tan\theta)}{S}$$

$$\simeq 500{,}000$$

- RECIPROCAL DISPERSION:

$$= \frac{\Delta\lambda}{\Delta\ell} = \frac{d\cos\theta}{mF}$$

$\simeq$ 0.5 Å/mm at 2600Å

- WAVE LENGTH RANGE: 1900Å – 3600Å
- RECORDING SYSTEM: Photographic

Many-body Effects

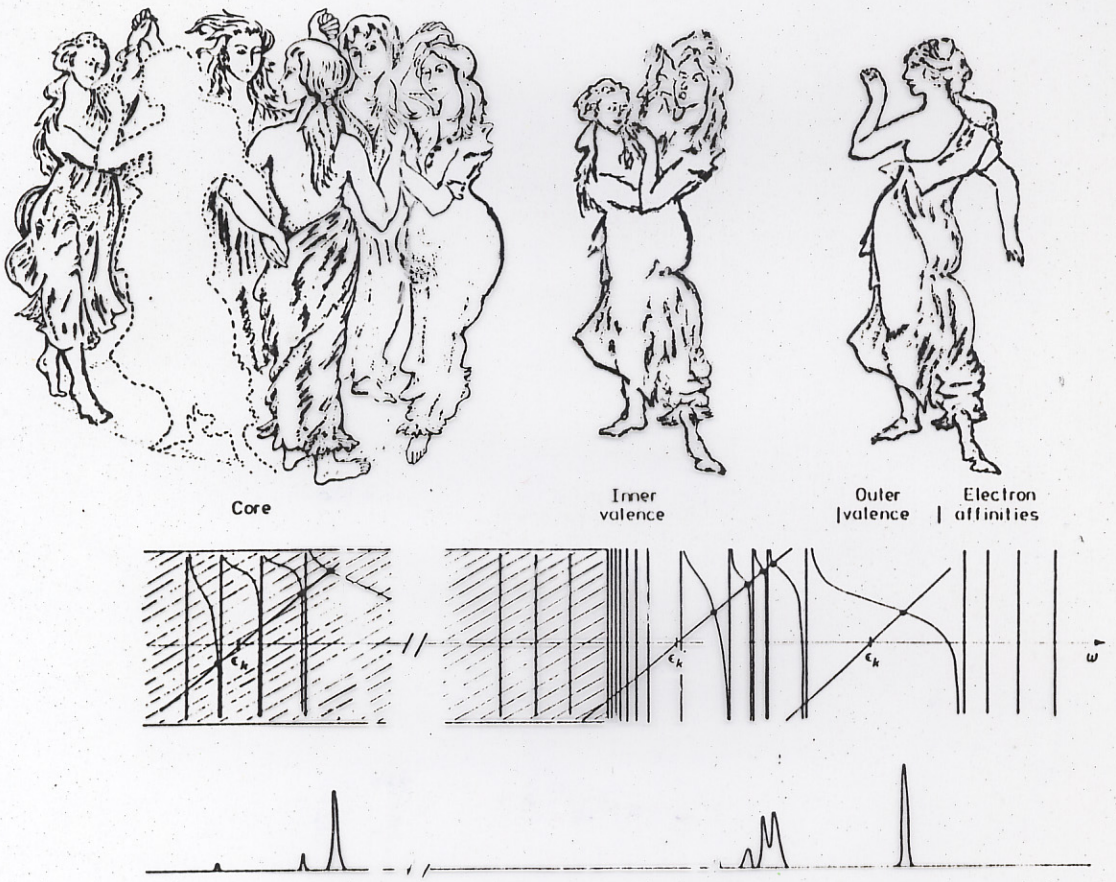

A schematic plot of the self-energy part $\Sigma_{kk}(\omega)$ and its poles as a function of energy ϵ. The energies which correspond to peaks in the ionisation spectrum are given by the intersection points n of the straight line $y = \omega - \epsilon_k$ with $\Sigma_{kk}(\omega)$.

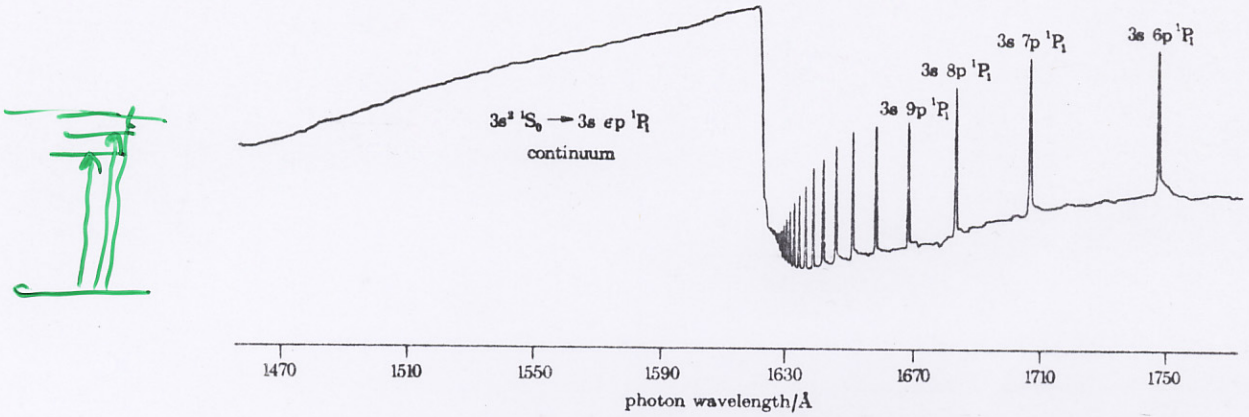

FIGURE 2. The principal series due to excitation of $3s^2\ ^1S_0 \longrightarrow 3s\,np\ ^1P_1$ in Mg I, showing the sudden onset and uniform decrease of continuous absorption above the first ionization threshold. The apparently discontinuous rise at threshold is an artefact, as traces at higher magnification reveal. The decrease in continuous absorption with decreasing wavelength persists until the structures of figure 3 are reached.

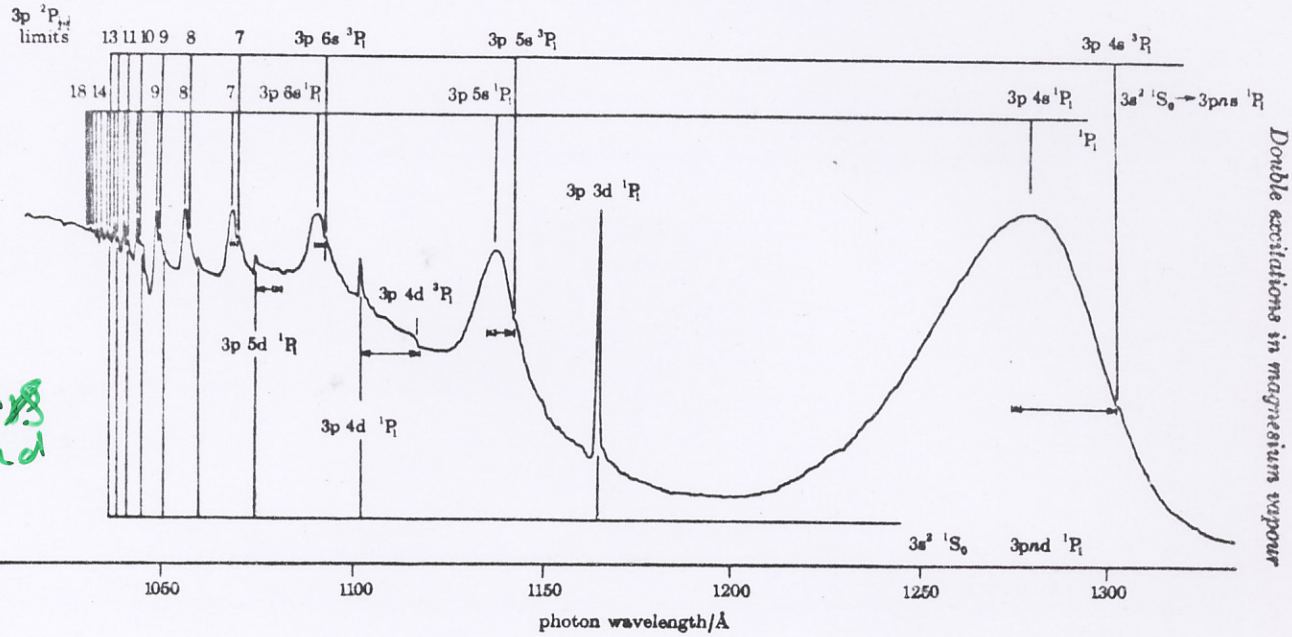

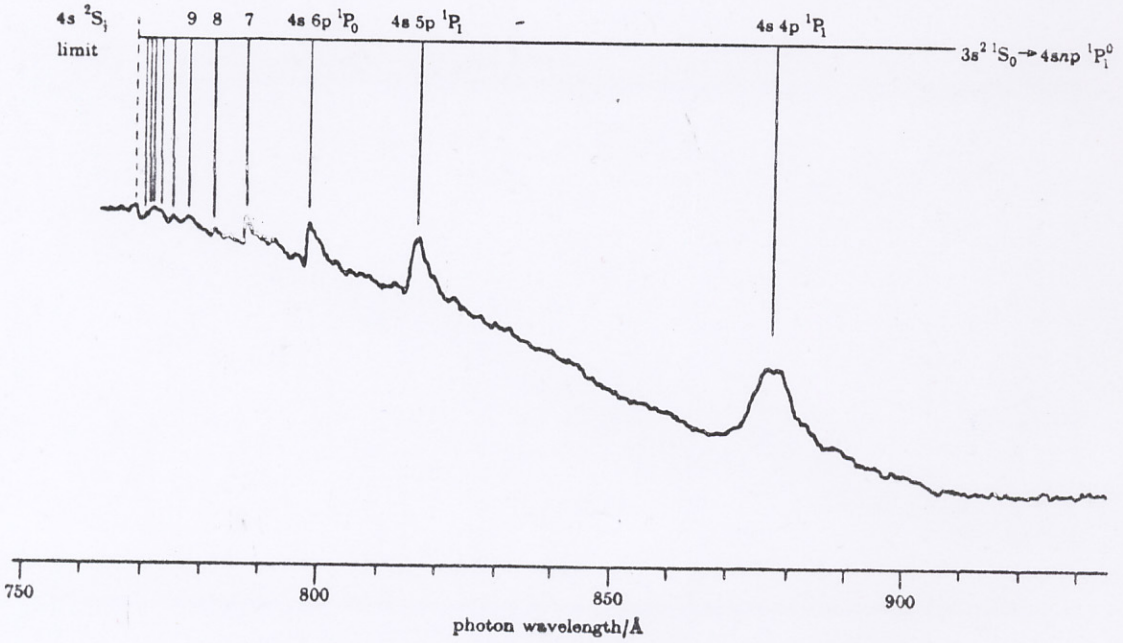

FIGURE 4. Showing the series due to double excitation $3s^2\ ^1S_0 \longrightarrow 4s\,np\ ^1P_1^0$ of Mg I.

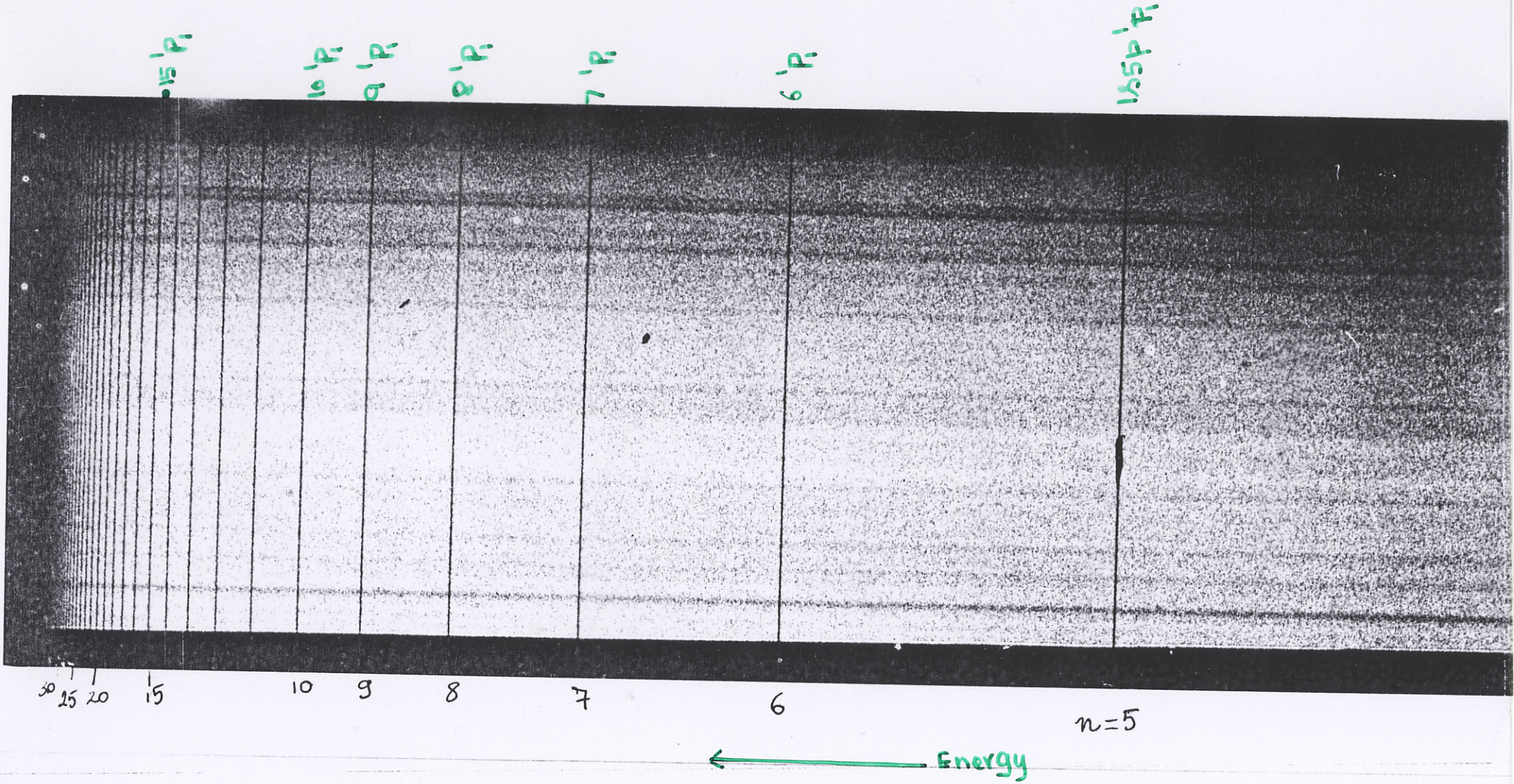
15 ¹P₁
10 ¹P₁
9 ¹P₁
8 ¹P₁
7 ¹P₁
6 ¹P₁
1s5p ¹P₁
50
25
20
15
10
9
8
7
6
n=5
Energy

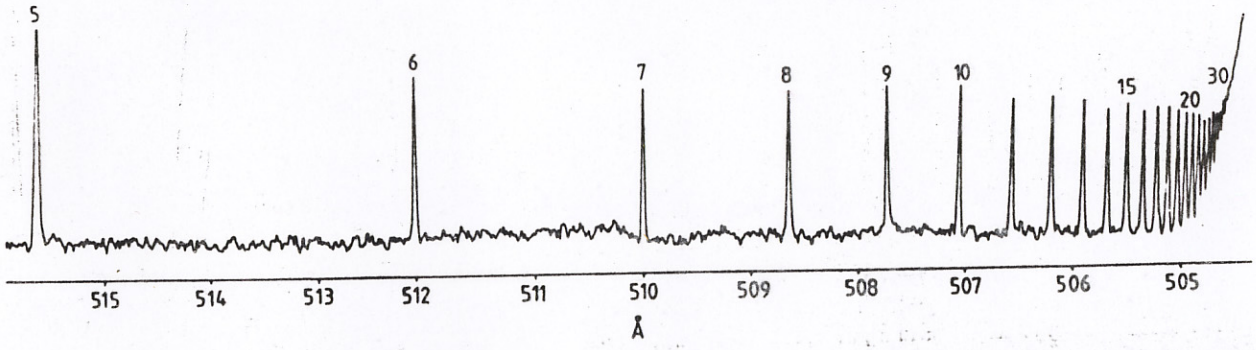

The principal series of helium from 516 to 504 Å (absorption plotted against wavelength).

Baig etal J. Phys. B. (UK) 1984

Spectrum of helium

Absorption Spectrum of Helium
"Doubly excited States"

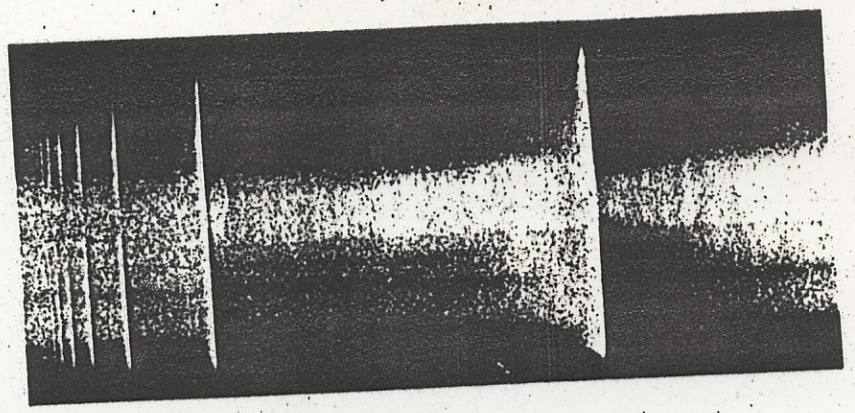

Photograph

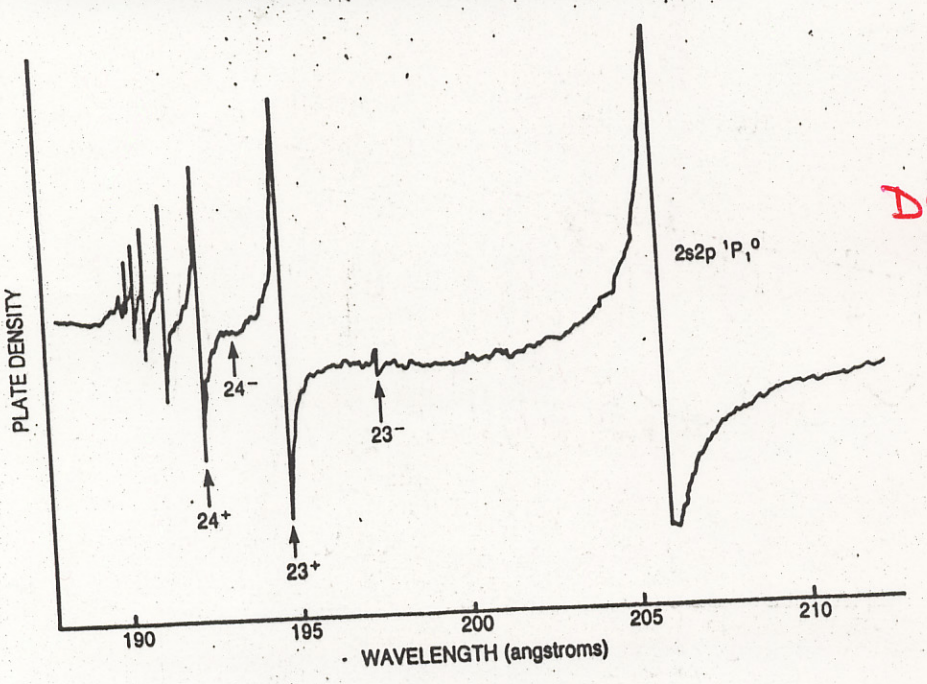

Densitometeric Trace

Double Excitation in Helium

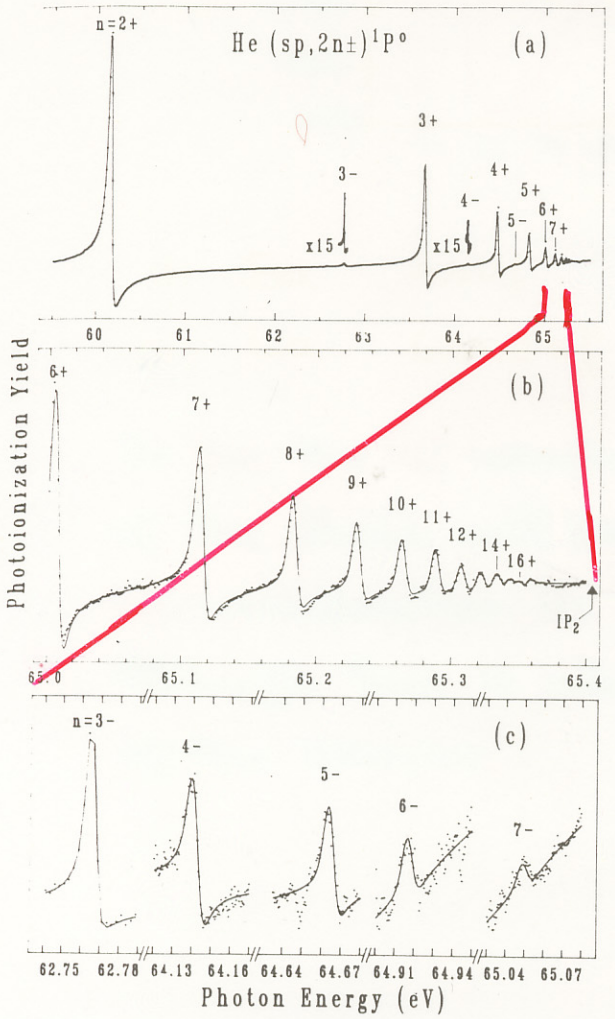

FIG. 1. Autoionizing states of double-excited He below the $N=2$ threshold (IP_2) of He: (a) overview, (b) magnification of the $n \geq 6$ region, and (c) "$2n-$" states.

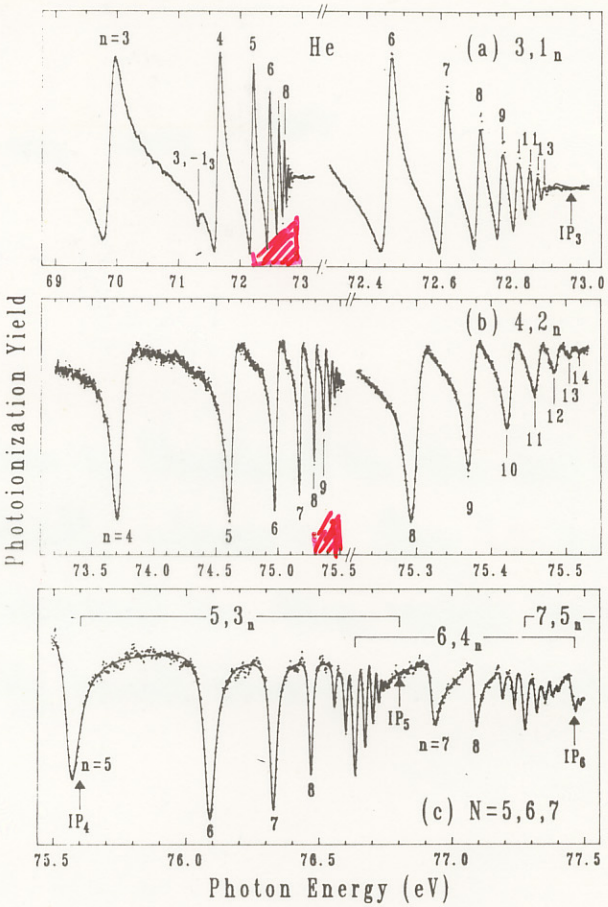

FIG. 2. Autoionizing states of He: (a) below the $N=3$ threshold (IP_3), (b) below the $N=4$ threshold (IP_4), and (c) below the $N=5$ and 6 thresholds (IP_5, IP_6). The high-n regions are shown magnified on the right-hand sides in (a) and (b). Note the overlapping of series in (c).

RYDBERG ATOMS

Property	General formula	Rydberg Atom $n = 30$
Size	$d = a_0 n^2$	10^3 Å
Binding Energy	$E_n = -R/n^2$	10^{-2} eV
Transition Energy $\Delta n = 1$	$\Delta E = 2R/n^3$	10^{-3} eV $\hat{=}$ 10 cm^{-1}
Life Time	$\tau \propto n^{+3}$	$30 \cdot 10^{-6}$ s.
Geometric Cross section (cm^2)	$\sigma = \pi a_0 n^4$	7.14×10^{-11}

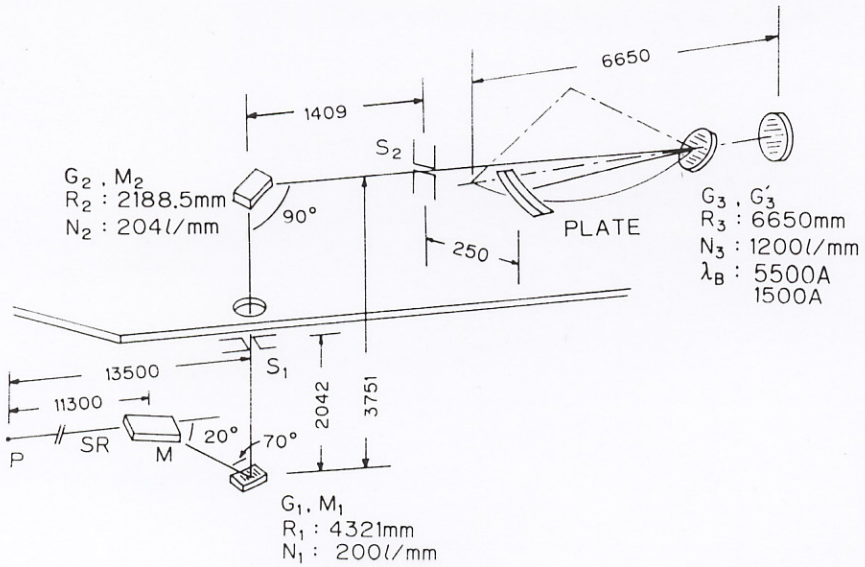

Fig. 1. Schematic diagram of the optical system of 6VOPE. The lengths are in mm. R_i is the diameter of ith optical element, N_i the groove density of ith grating, and λ_B the blaze wavelength of G_3/G'_3.

With this arrangement a desired wavelength portion of SR can be sorted out by a simple rotation of G_1 and adjustment of the width of S_1, and the properly filtered SR can be counter-dispersed to have zero dispersion and focused on S_2 by a simple rotation of G_2.

3. 6VOPE and its performance

The beamline and the predisperser system are ultra-high vacuum compatible, whereas the main instrument is allowed to use O-rings to facilitate the use of rather complex mechanisms inside the vacuum chamber. The vacuum system is equipped with turbo molecular pumps backed by a mechanical booster and/or a rotary pump, ion pumps, a Ti sublimation pump, pneumatic valves, and usual vacuum components.

6VOPE has three different operational modes: spectrograph, focal plane scanning, and monochromator modes. The spectrograph mode can easily be converted into the focal plane scanning mode by moving the cassette holder sidewise and by bringing the computer controlled exit slit/absorption cell/photomultiplier unit into the focal position, without braking the vacuum. 6VOPE can also be used as a monochromator by replacing the G_1 and G_2 with concave mirrors whose radii of

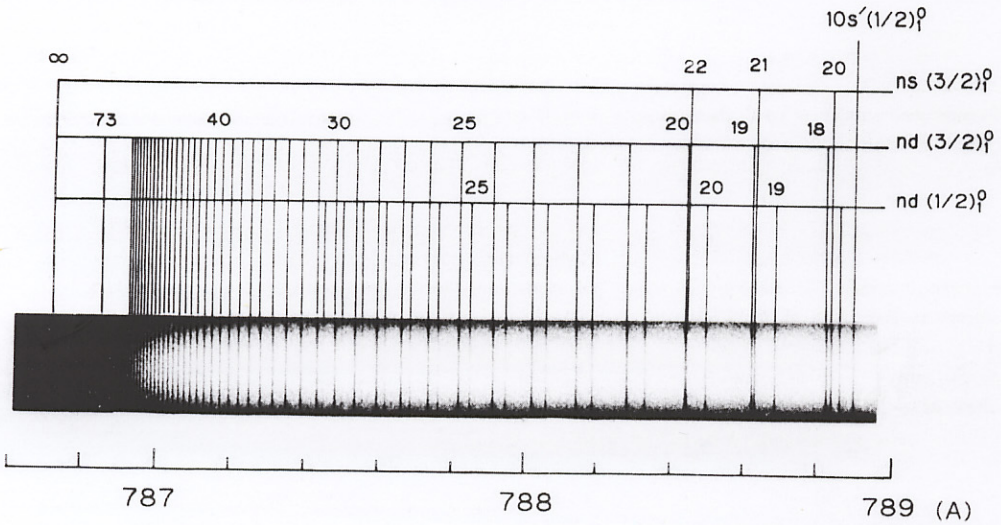

Fig. 2. Absorption spectrum of Ar taken in the 7th order.

NEON

SPECTRUM OF Ne

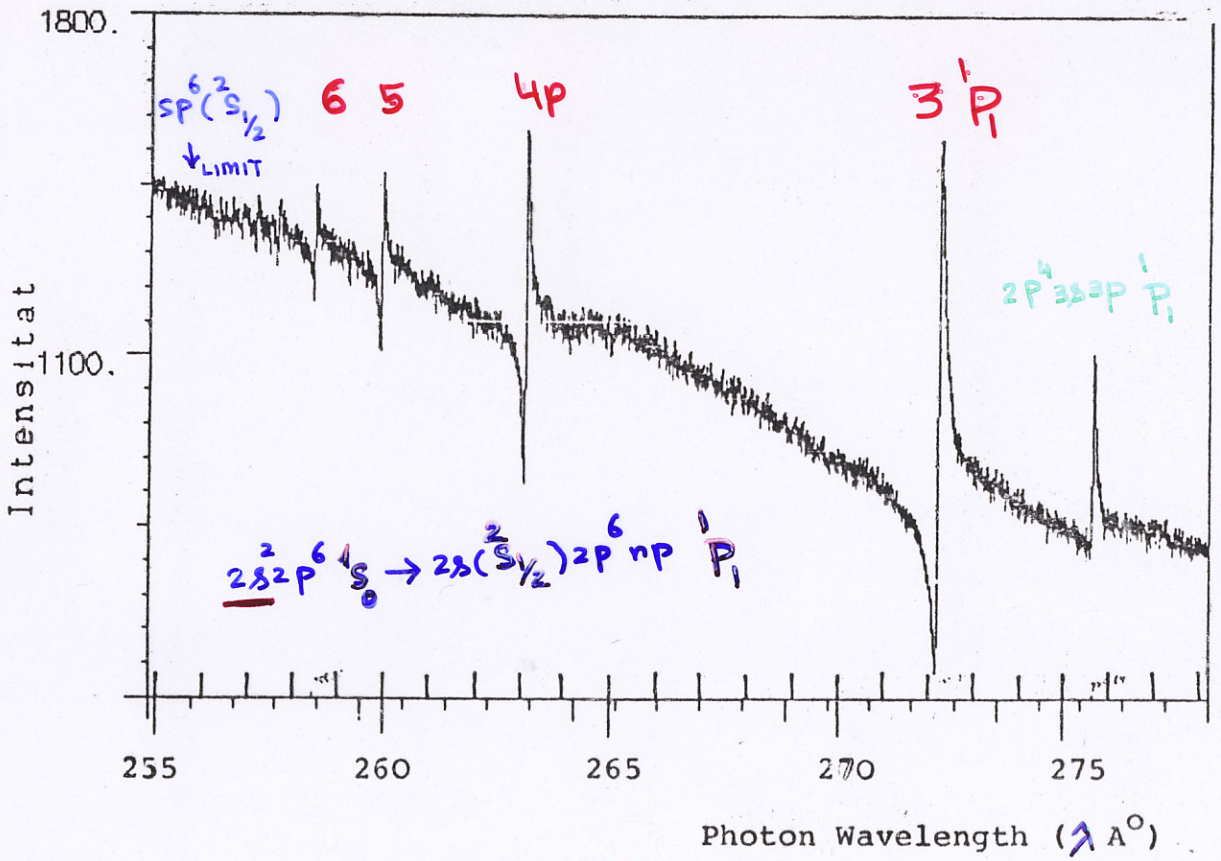

ABSORPTION SPECTRUM OF MgI.

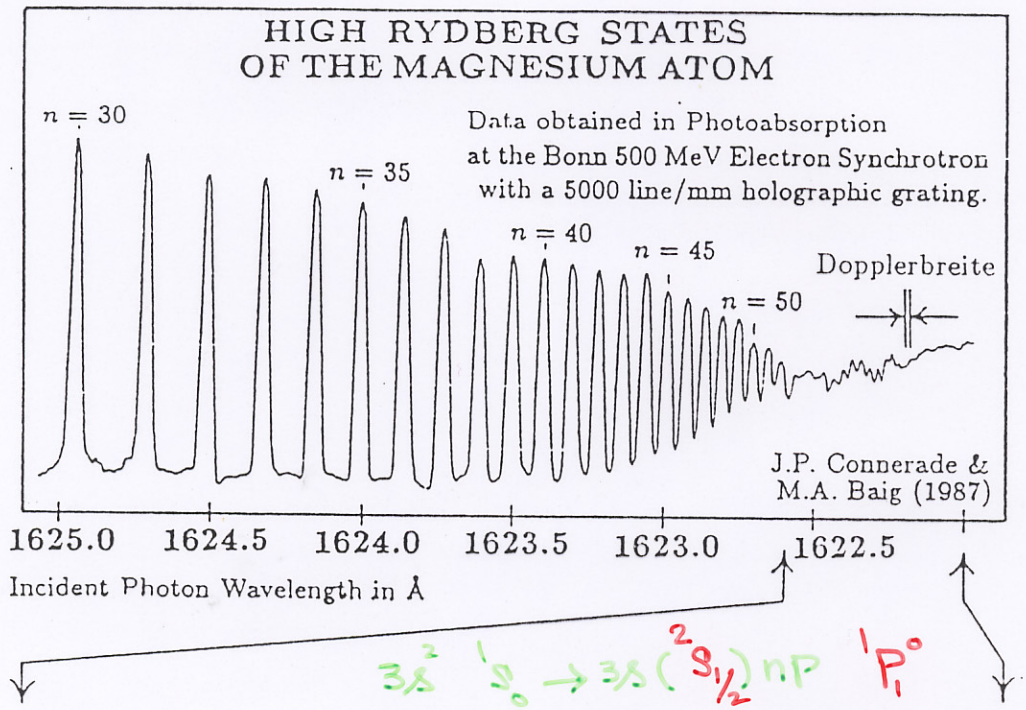

$3s^2\ {}^1S_0 \rightarrow 3s({}^2S_{1/2})nP\ {}^1P_1^\circ$

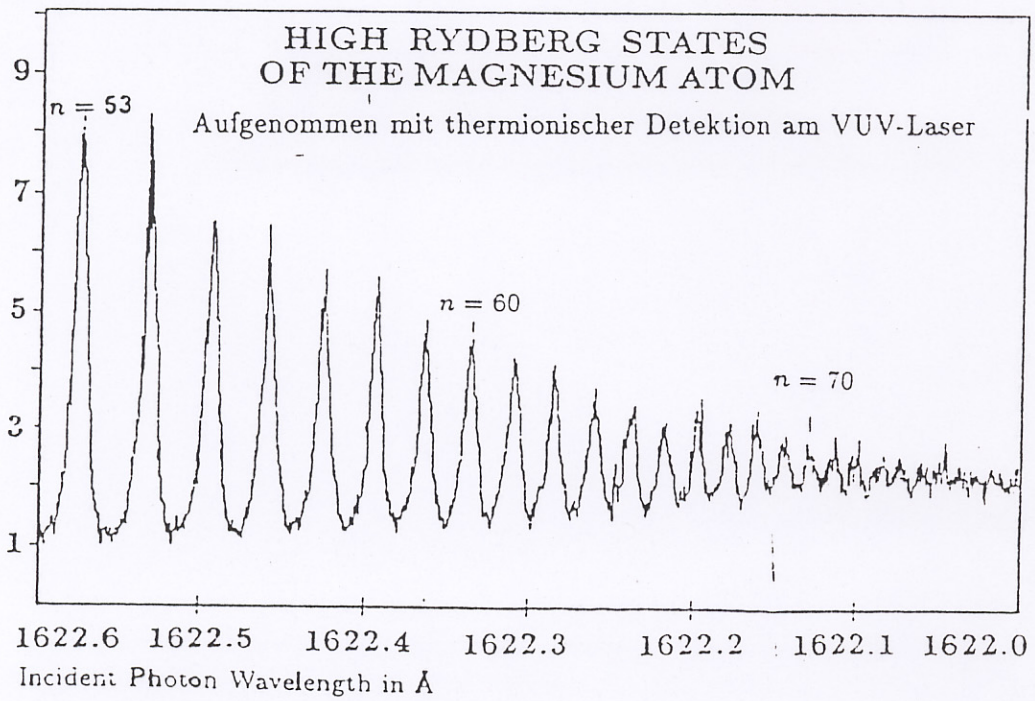

6000 line/mm. Grating
0.44 Å/mm. (Frist order)

Ground state:

$5d^{10}6s^2 6p\ {}^2P_{\frac{1}{2},\frac{3}{2}}$ (7792.7 cm^{-1})

(i) $\rightarrow 6s^2\ ns\ {}^2S_{1/2}$ $(12<n<40)$

$nd\ {}^2D_{3/2}$ $(12<n<70)$

I.P :

49264.2	± 2 cm^{-1}	Moore (1958)
49265.9	± 0.3 cm^{-1}	Penkin & Shabanova (1965)
49266.7	± 0.2 cm^{-1}	Reeves, Garton (1965)
49266.62	± 0,02 cm^{-1}.	Present work.

$T_\alpha (F=1 \rightarrow F=2) = 49265.91 \pm 0{,}02\ cm^{-1}$
$T_\alpha (F=0 \rightarrow F=1) = 49266.62 \pm 0{,}02\ cm^{-1}$.

HFS:

0.711	Tl^{205}	Flusberg et.al. 1976
0.704	Tl^{203}	
0.710 ± 0,007 cm^{-1}.		Present work.

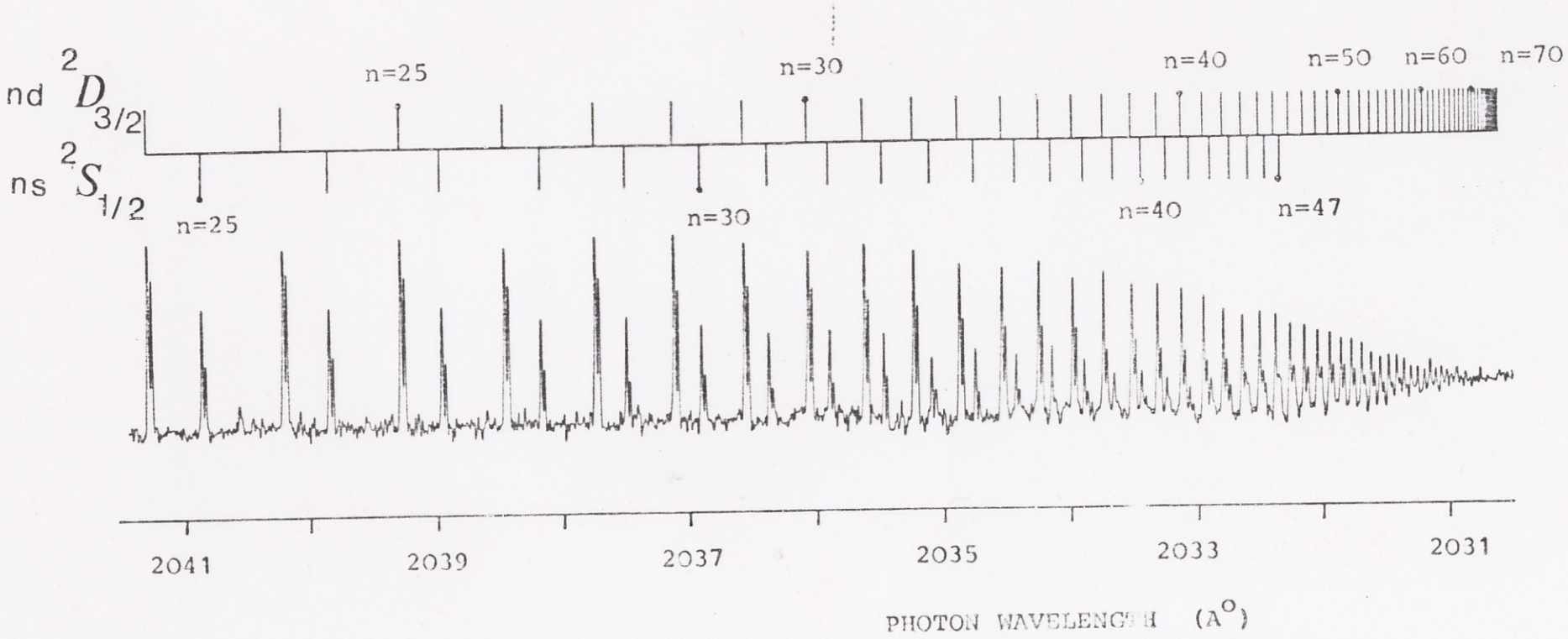

Baig & Connerade 1985

FIGURE (1)

Alkali Elements:

Inner Shell Excitation

$mp^6(m+1)s \longrightarrow mp^5(m+1)s$

$\longrightarrow (^3P_2)$ ns $[2]_{3/2}$
nd $[0],[1],[2]$

$\longrightarrow (^3P_1)$ ns $[1]_{1/2,3/2}$
nd $[1],[2]$

$\longrightarrow (^3P_0)$ ns $[0]_{1/2}$
nd $[2]_{3/2}$

$\longrightarrow (^1P_1)$ ns $[1]_{1/2,3/2}$
nd $[1],[2]_{3/2}$

Effective Quantum Numbers:

Na	7d =	6.72	8s =	6.35
K	9d =	7.55	10s =	7.55
Rb	10d =	7.40	11s =	7.68
Cs	11d =	7.36	12s =	7.75

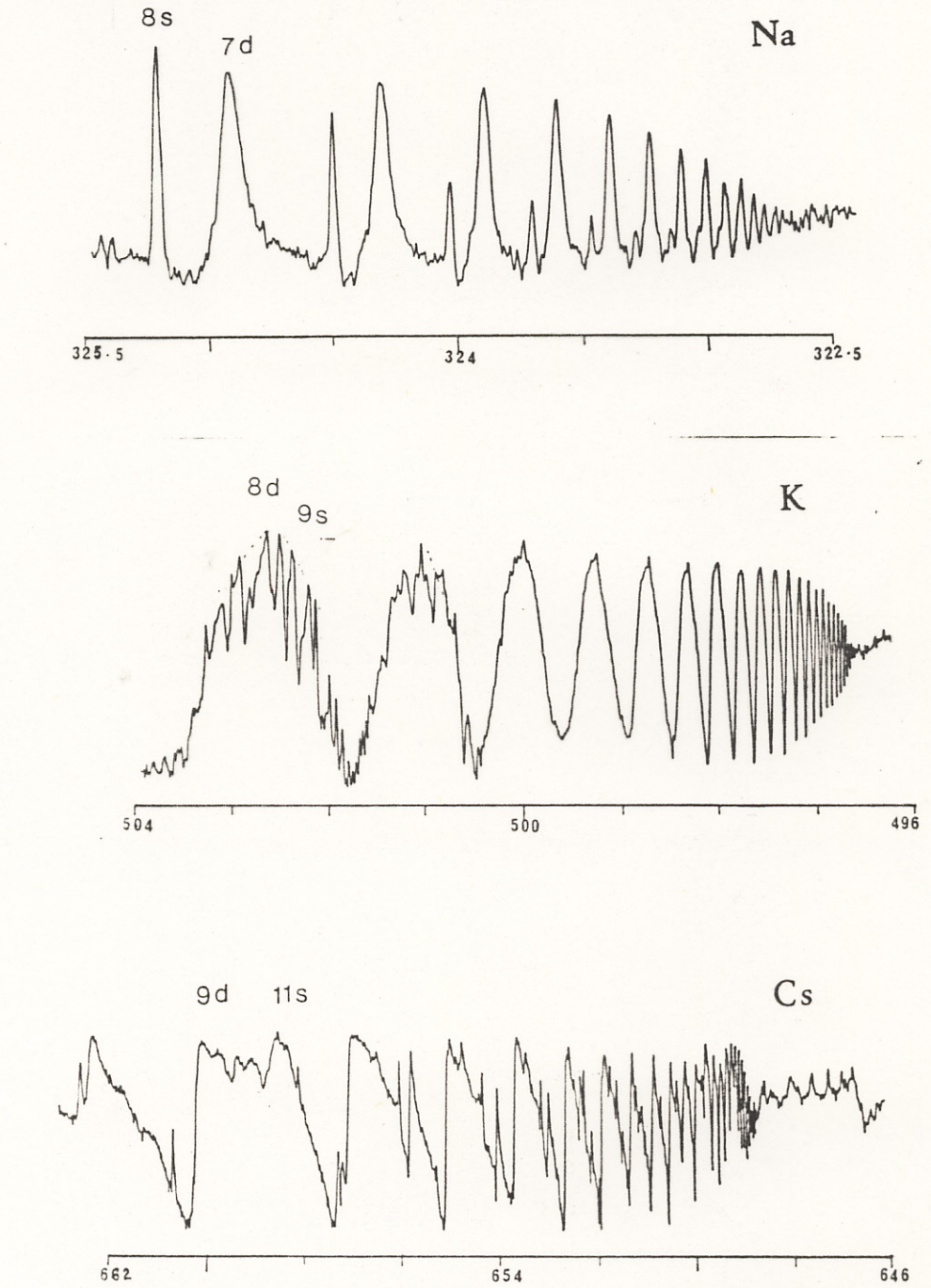
8s
7d
Na
325·5
324
322·5
8d
9s
K
504
500
496
9d
11s
Cs
662
654
646

Jck-Coupling Scheme

- $\{[[\{(\ell_1, s_1)\, j_c\}\, \ell_2, k]\, s_2\}_J$

- $3d^9 4s ({}^3D)\, 6p$
  - $({}^3D_3)\, 6p \quad [2]^\circ_{3/2}$
  - $({}^3D_3)\, 4f \quad [0]^\circ_{1/2}, \; [1]^\circ_{1/2,3/2}$
  - $({}^3D_2)\, 6p \quad [2]^\circ_{3/2}, \; [1]^\circ_{1/2,3/2}$
  - $({}^3D_2)\, 4f \quad [2]^\circ_{3/2}, \; [1]^\circ_{1/2,3/2}$
  - $({}^3D_1)\, 6p \quad [0]^\circ_{1/2}, \; [1]^\circ_{1/2,3/2}, \; [2]^\circ_{3/2}$
  - $({}^3D_1)\, 4f \quad [2]^\circ_{3/2}$

Baig et.al Phys. Rev. (1992)

$4d^9 5s(^3D_{3,2,1})7p$& 4f-Configurations

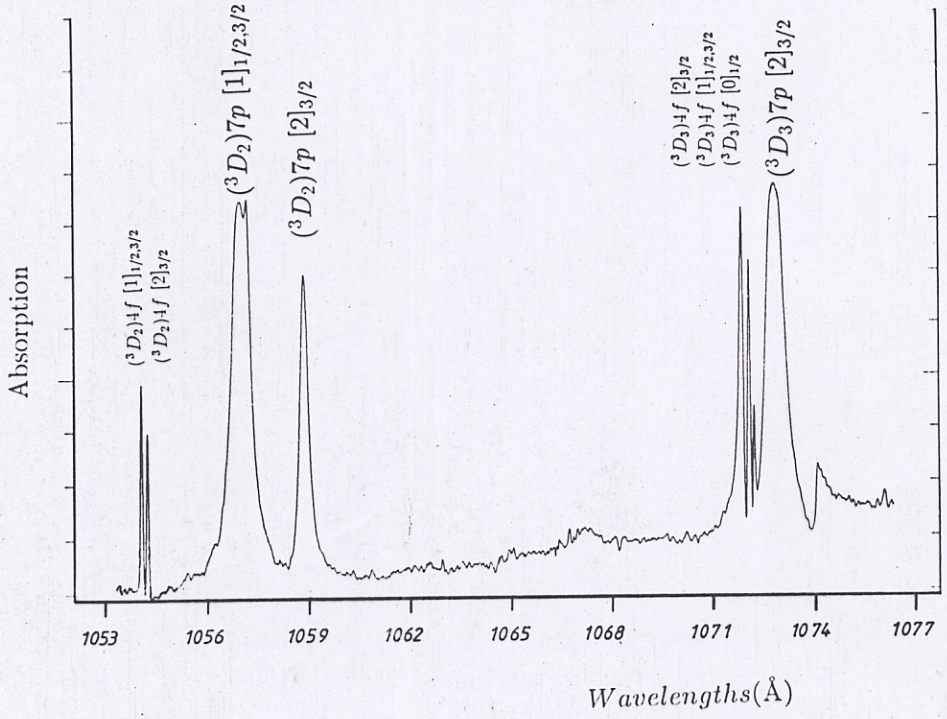

Baig etal. Phys. Rev (1992)

$3d^9 4s(^3D_{3,2,1})6p$& 4f-Configurations

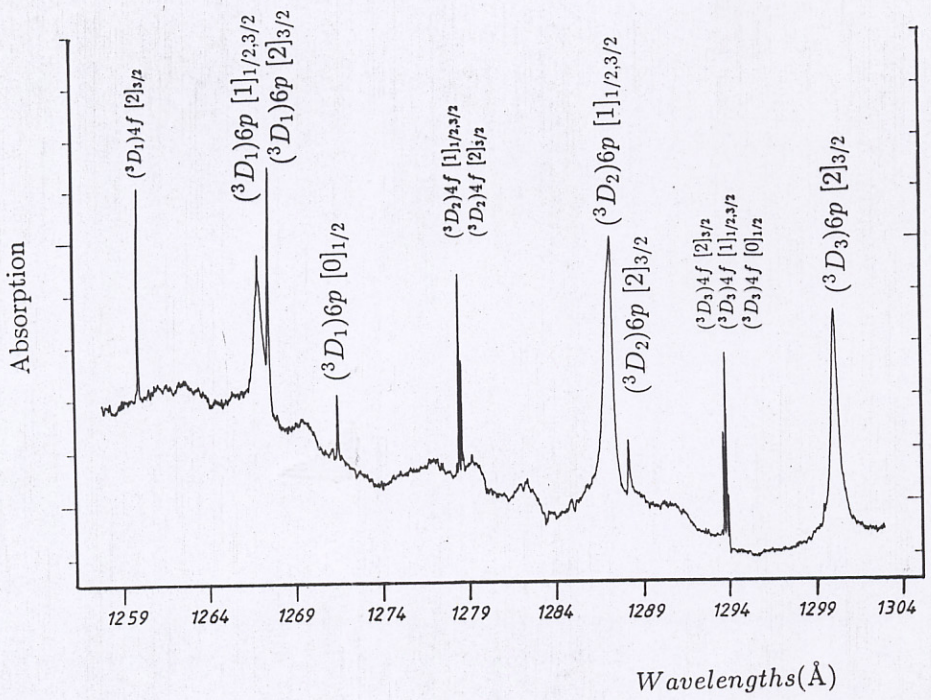

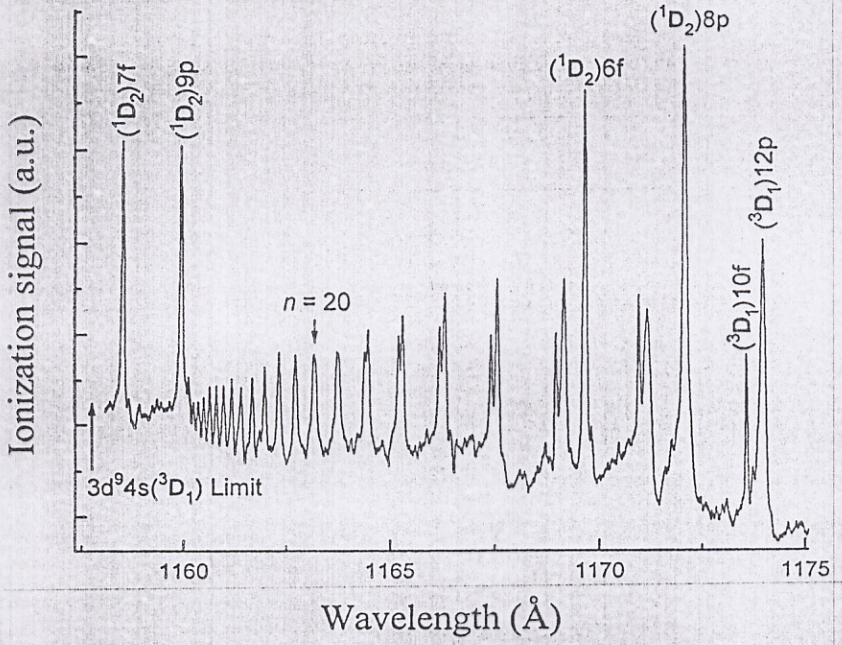
Ionization signal (a.u.)
(1D2)7f
(1D2)9p
(1D2)6f
(1D2)8p
(3D1)10f
(3D1)12p
n = 20
3d94s(3D1) Limit
1160
1165
1170
1175
Wavelength (Å)

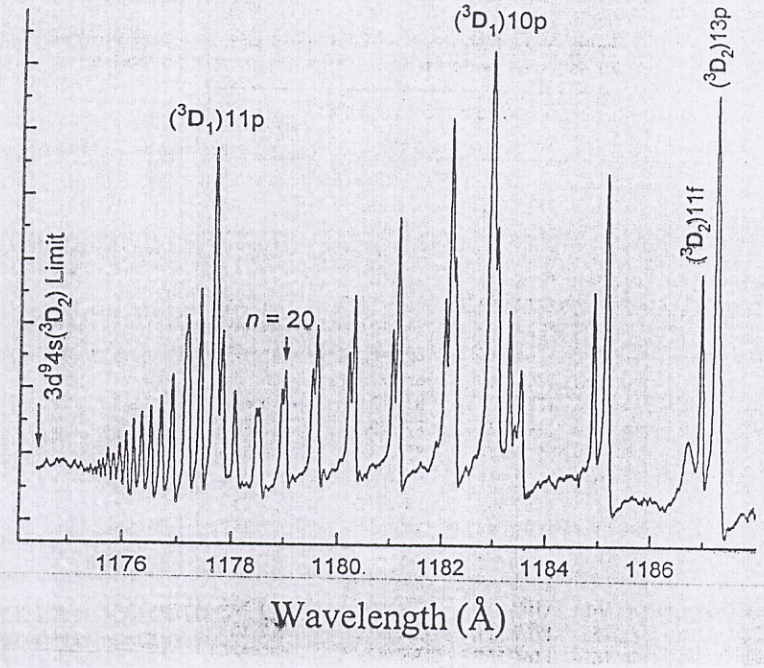
(3D1)10p
(3D2)13p
(3D1)11p
(3D2)11f
n = 20
3d94s(3D2) Limit
1176
1178
1180
1182
1184
1186
Wavelength (Å)

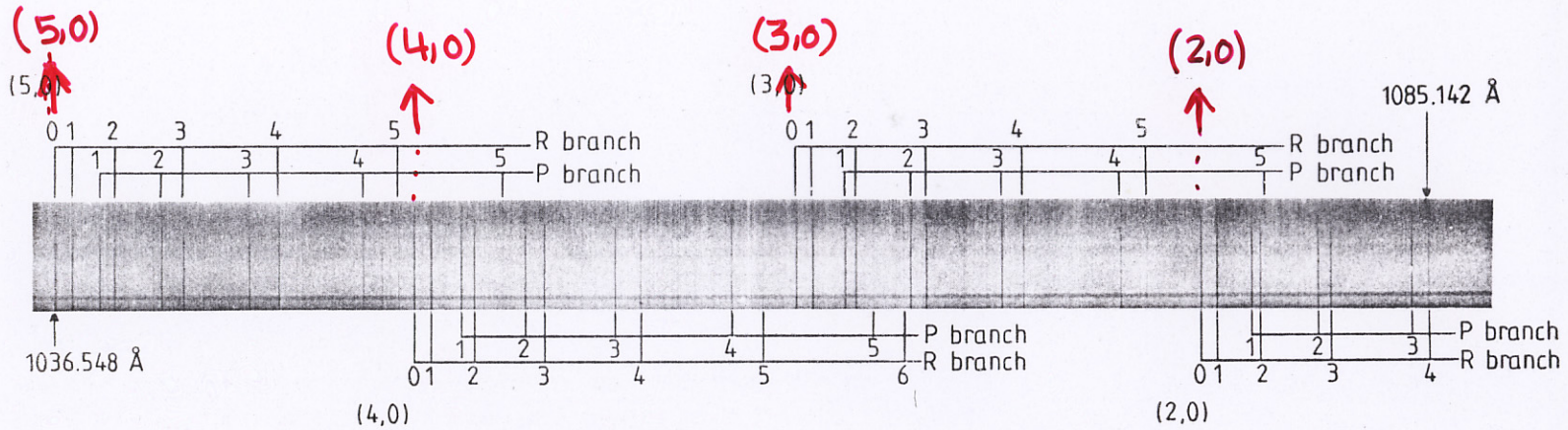

Figure 1. The absorption spectrum of H_2 between 1036 and 1085 Å, showing the (2, 0), (3, 0), (4, 0) and (5, 0) vibrational bands of the $B\,^1\Sigma$–$X\,^1\Sigma$ system.

[facing p L810]

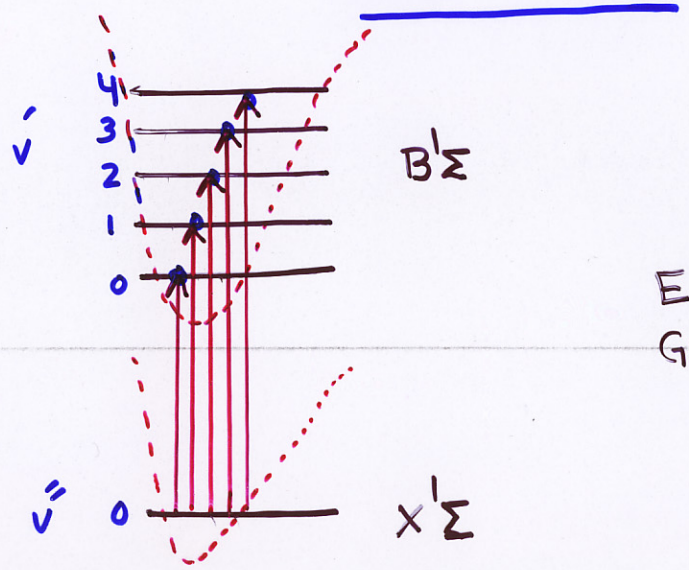

Baig et al (1985)

$$E(J) = B_v J(J+1) - D_v J^2(J+1)^2 + H_v J^3(J+1)^3$$

$$G(v) = \omega_e(v+\tfrac{1}{2}) - \omega_e x_e(v+\tfrac{1}{2})^2 + \omega_e y_e(v+\tfrac{1}{2})^3$$

24

QUASI-ATOMIC RYDBERG STATES

CH_3I

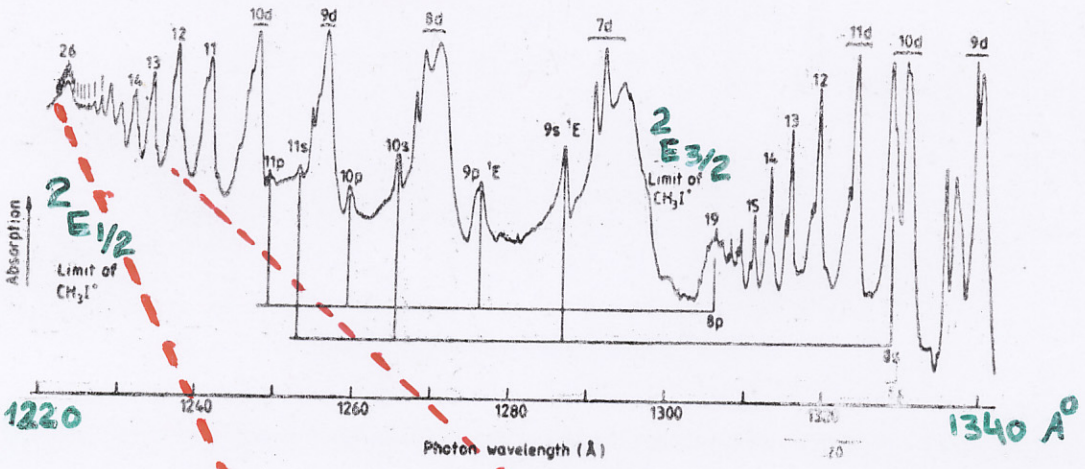

$(a\sigma)^2(e\pi)^4\ {}^1A_1 \longrightarrow (e\pi)^3({}^2E_{3/2})\ n\ell\lambda$

$\longrightarrow\ ({}^2E_{1/2})\ n\ell\lambda$

Spin Orbit Splitting = 5050 cm^{-1}.

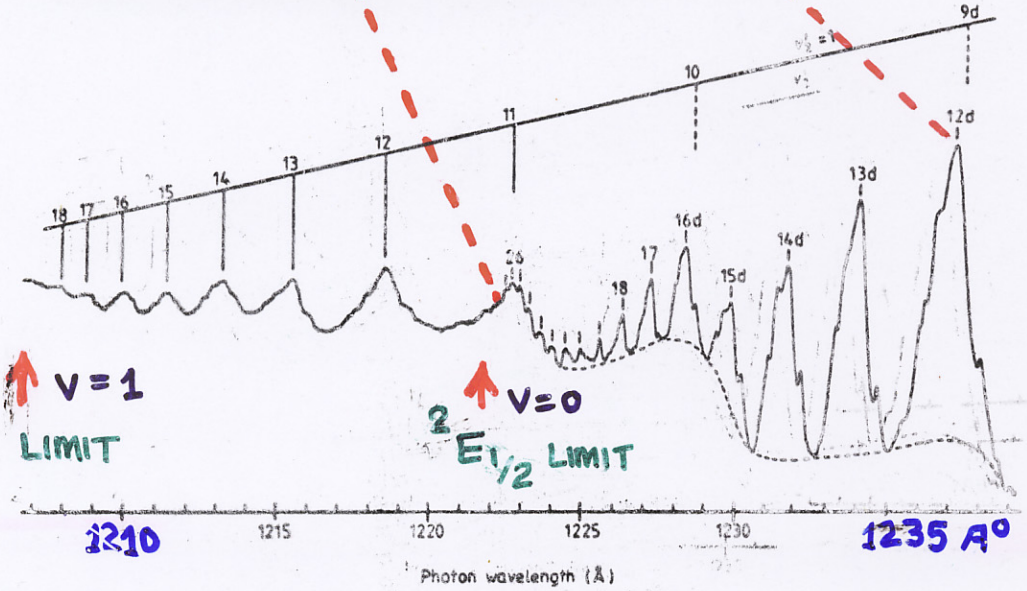

$5p^6\ {}^1S_0 \longrightarrow 5p^5({}^2P_{3/2})$ ns $[3/2]^0_1$; nd $[1/2]^0_1$; nd $[3/2]^0_1$

$\longrightarrow\ ({}^2P_{1/2})$ ns $[1/2]^0_1$; nd $[3/2]^0_1$

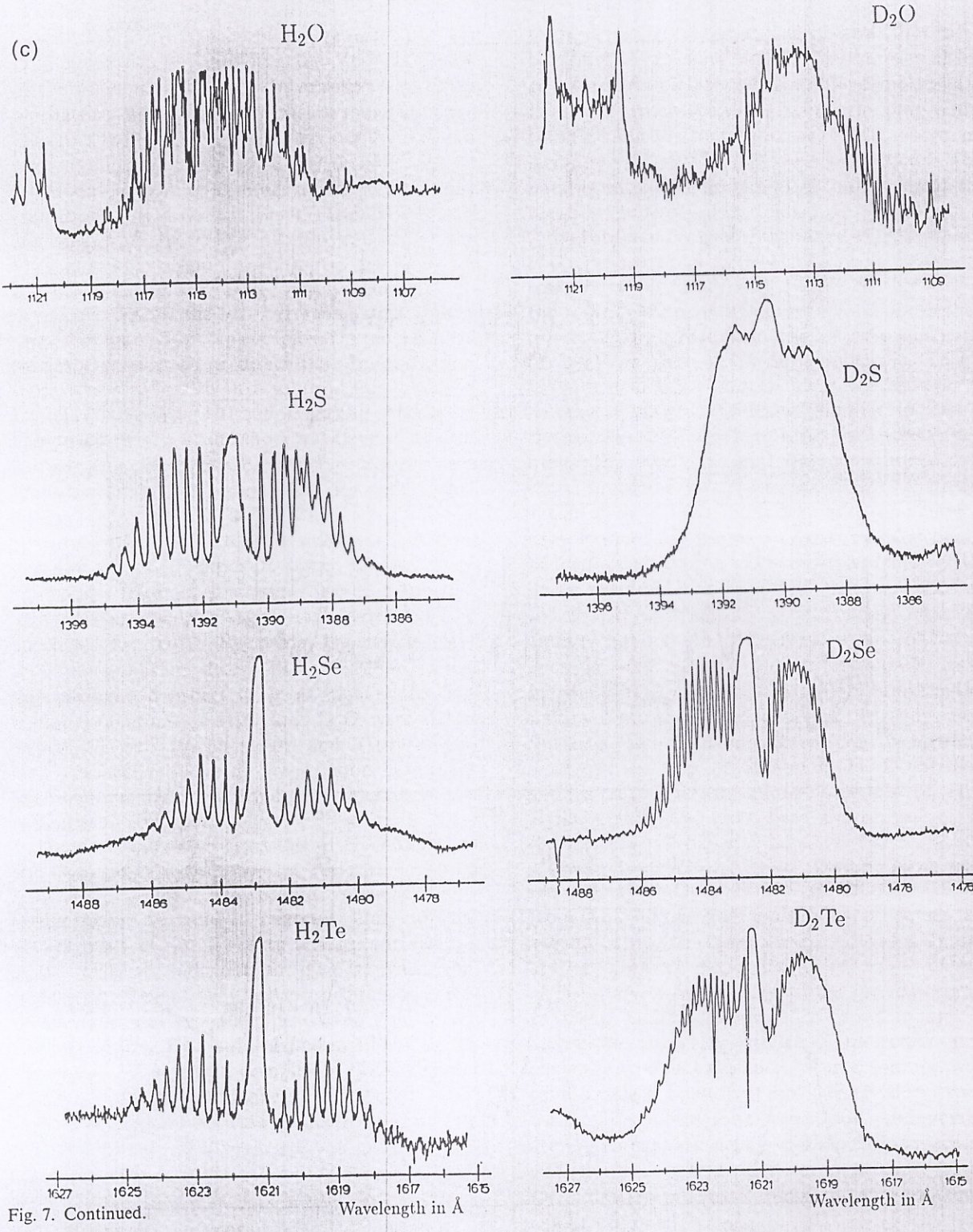

Fig. 7. Continued.

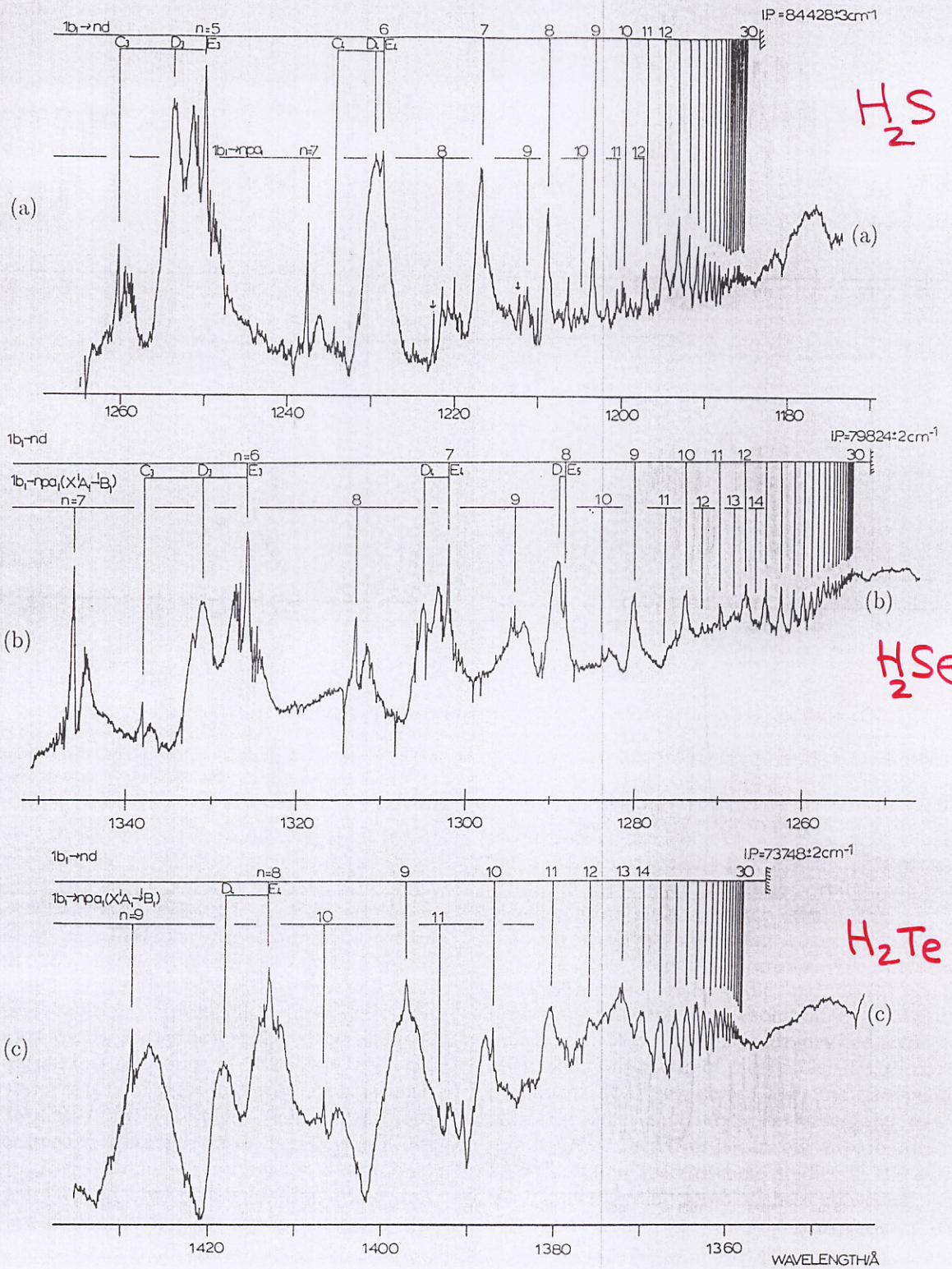
1b1→nd
n=5
6
7
8
9
10
11
12
30
C1
D1
E1
I.P.=84428±3cm-1
1b1→npa1
n=7
8
9
10
11
12
(a)
H2S
1260
1240
1220
1200
1180
1b1→nd
n=6
7
8
9
10
11
12
30
I.P.=79824±2cm-1
1b1→npa1(X1A1→1B1)
n=7
8
9
10
11
12
13
14
(b)
H2Se
1340
1320
1300
1280
1260
1b1→nd
n=8
9
10
11
12
13
14
30
I.P.=73748±2cm-1
1b1→npa1(X1A1→1B1)
n=9
10
11
(c)
H2Te
1420
1400
1380
1360
WAVELENGTH/Å

Autoionization

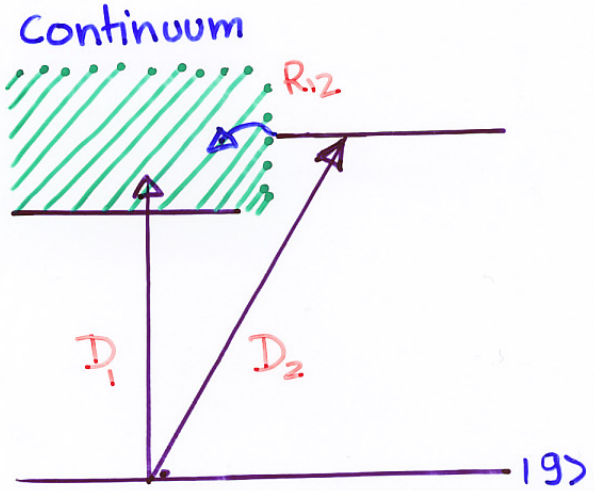

Line Profile

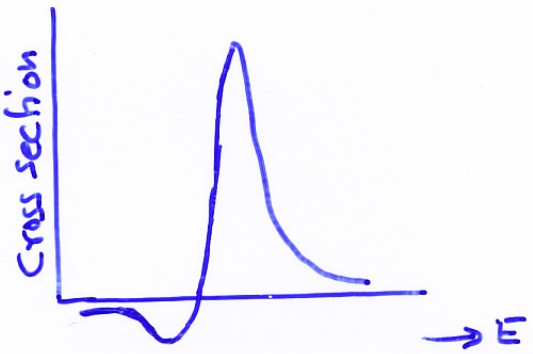

$$\sigma = K \frac{[D_1 \tan^2 \pi(\nu_2 + \delta_2) - D_2 R_{12}]^2}{\tan^2 \pi(\nu_2 + \delta_2) + R_{12}^4}$$

$$\Gamma = \frac{4 R_y R_{12}^2}{\pi \nu_2^3} \quad cm^{-1}$$

$$\sigma = \sigma_1 \left(\frac{(\varepsilon + q)^2}{1 + \varepsilon^2}\right) + \sigma_b \quad ; \quad \varepsilon = \frac{2(E - E_R)}{\Gamma}$$

$$\varepsilon = \tan \pi (\nu_2 + \delta_2) / R_{12}^2$$

$$q = - \frac{D_2}{D_1 R_{12}}$$

Photoionization cross section

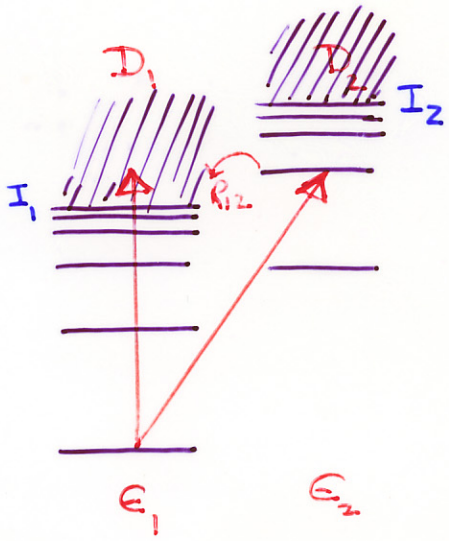

$$I_1 < E < I_2$$

channel 1 $\Rightarrow$ open

channel 2 $\Rightarrow$ close

$$\sigma = k \left| \sum_i a_i D_i \right|^2$$

$$= k \left| a_1 D_1 + a_2 D_2 \right|^2$$

$$= a_1^2 k \left| D_1 + \left(\frac{a_2}{a_1}\right) D_2 \right|^2$$

$\epsilon_i = \tan \pi(\nu_i + \mu_i)$

$a_i = \cos \pi(\nu_i + \mu_i) A_i$

$$\begin{bmatrix} \epsilon_1 & R_{12} \\ R_{12} & \epsilon_2 \end{bmatrix} \begin{bmatrix} a_1 \\ a_2 \end{bmatrix} = 0$$

$$\therefore (\epsilon_1 \epsilon_2)^2 = R_{12}^4$$

$$\left(\frac{a_2}{a_1}\right) = -\frac{R_{12}}{\epsilon_2}$$

Substituting the value of $\left(\frac{a_2}{a_1}\right)$

$$\sigma = a_1^2 k \left| D_1 - \frac{R_{12}}{\epsilon_2} D_2 \right|^2$$

Substituting the value of a_1^2

$$\sigma = k \cdot \frac{A_1^2}{1+\epsilon_1^2} \left| D_1 - R_{12} \cot \pi(\nu_2 + \mu_2) D_2 \right|^2$$

eliminating ϵ_1 in this relation

$$\sigma = k \frac{A_1^2}{1 + \frac{R_{12}^4}{\epsilon_2^2}} \left| D_1 - R_{12} \cot \pi(\nu_2 + \mu_2) D_2 \right|^2$$

Since channel 1 is open, therefore $A_1^2 = 1$

$$\sigma = \frac{k}{1 + R_{12}^4 \cot^2 \pi(\nu_2 + \mu_2)} \left| D_1 - R_{12} D_2 \cot \pi(\nu_2 + \mu_2) \right|^2$$

$$\boxed{\sigma = k \cdot \frac{\left[D_1 - R_{12} \cot \pi(\nu_2 + \mu_2) \right]^2}{1 + R_{12}^4 \cot^2 \pi(\nu_2 + \mu_2)}}$$

(Baig & Bhatti, 1994)

Intensities in the Discrete Region

$$\sigma = |\Sigma a_i D_i|^2$$

Normalization condition

$$1 = \Sigma A_i^2 \nu_i^3 = \Sigma a_i^2 (1+\epsilon_i^2)\nu_i^3$$

For the Two-Channel Case

$$\sigma = |a_1 D_1 + a_2 D_2|^2$$

$$= a_1^2 \left| D_1 + \frac{a_2}{a_1} D_2 \right|^2$$

Normalization condition

$$a_1^2(1+\epsilon_1^2)\nu_1^3 + (1+\epsilon_2^2)\nu_2^3 a_2^2 = 1$$

or

$$\frac{1}{a_1^2} = (1+\epsilon_1^2)\nu_1^3 + (1+\epsilon_2^2)\nu_2^3 \frac{a_2^2}{a_1^2}$$

The Two-Channel MQDT eq.

$$\begin{pmatrix} \epsilon_1 & R \\ R & \epsilon_2 \end{pmatrix} \begin{pmatrix} a_1 \\ a_2 \end{pmatrix} = 0$$

$\det = 0$ gives $\epsilon_1 \epsilon_2 = R^2$

$$\epsilon_1 a_1 + R a_2 = 0 \Rightarrow \frac{a_2}{a_1} = -\frac{\epsilon_1}{R}$$

$$I_n = \frac{|D_1 + D_2(-\frac{\epsilon_1}{R})|^2}{(1+\epsilon_1^2)\nu_1^3 + (1+\epsilon_2^2)\nu_2^3 (\frac{\epsilon_1^2}{R^2})}$$

$$I_n = \frac{|R D_1 - \epsilon_1 D_2|^2}{(1+\epsilon_1^2)\nu_1^3 R^2 + (1+\epsilon_2^3)\nu_2^3 \epsilon_1^2}$$

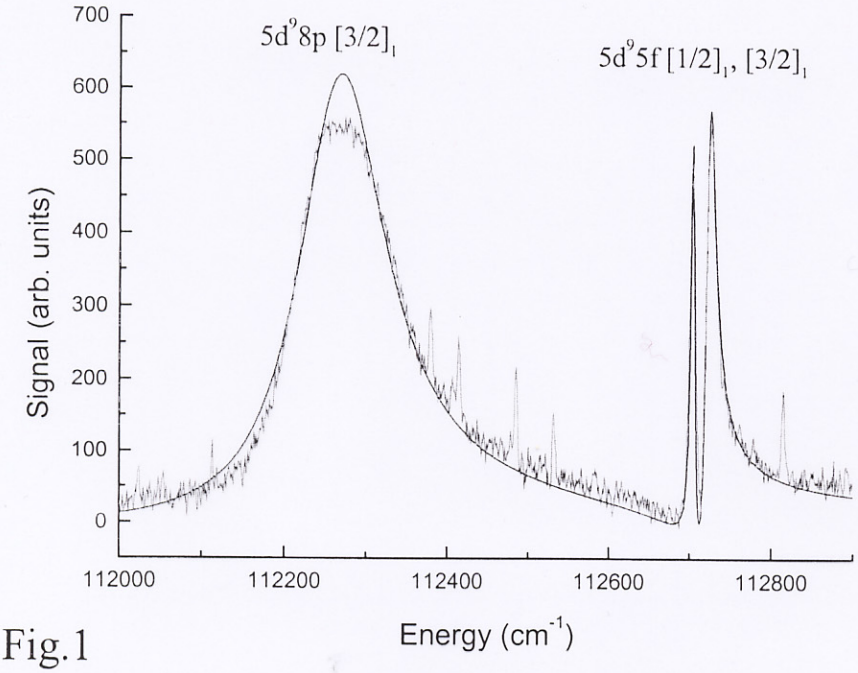
5d⁹8p [3/2]₁
5d⁹5f [1/2]₁, [3/2]₁
Signal (arb. units)
Energy (cm⁻¹)
700
600
500
400
300
200
100
0
112000
112200
112400
112600
112800

Fig.1

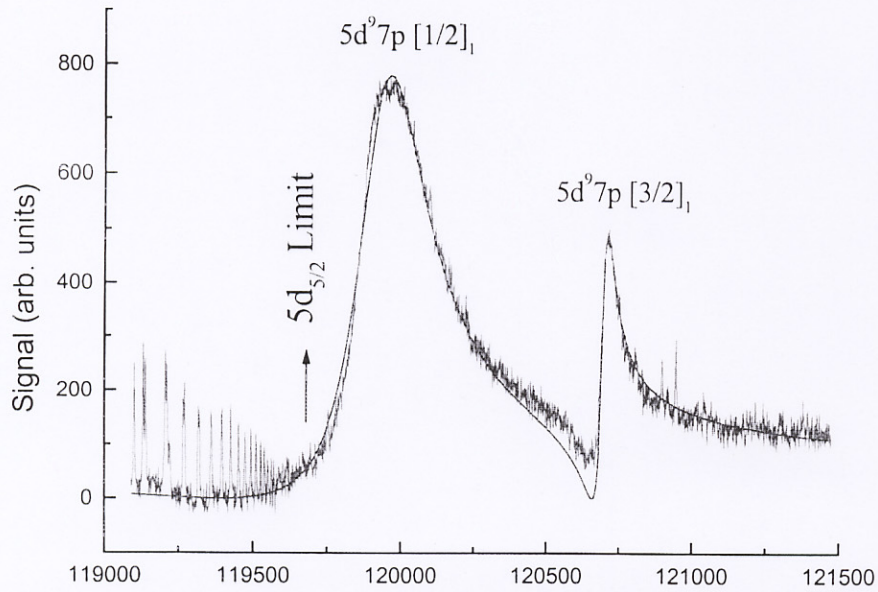
5d⁹7p [1/2]₁
5d⁹7p [3/2]₁
5d5/2 Limit
Signal (arb. units)
Energy (cm⁻¹)
800
600
400
200
0
119000
119500
120000
120500
121000
121500

Fig. 2

ABSORPTION SPECTRUM OF XeI.

Comparison between calculated and experimental profiles for a series of autoionising resonances in Xenon using the Seaton-Dubau (1982) formula.

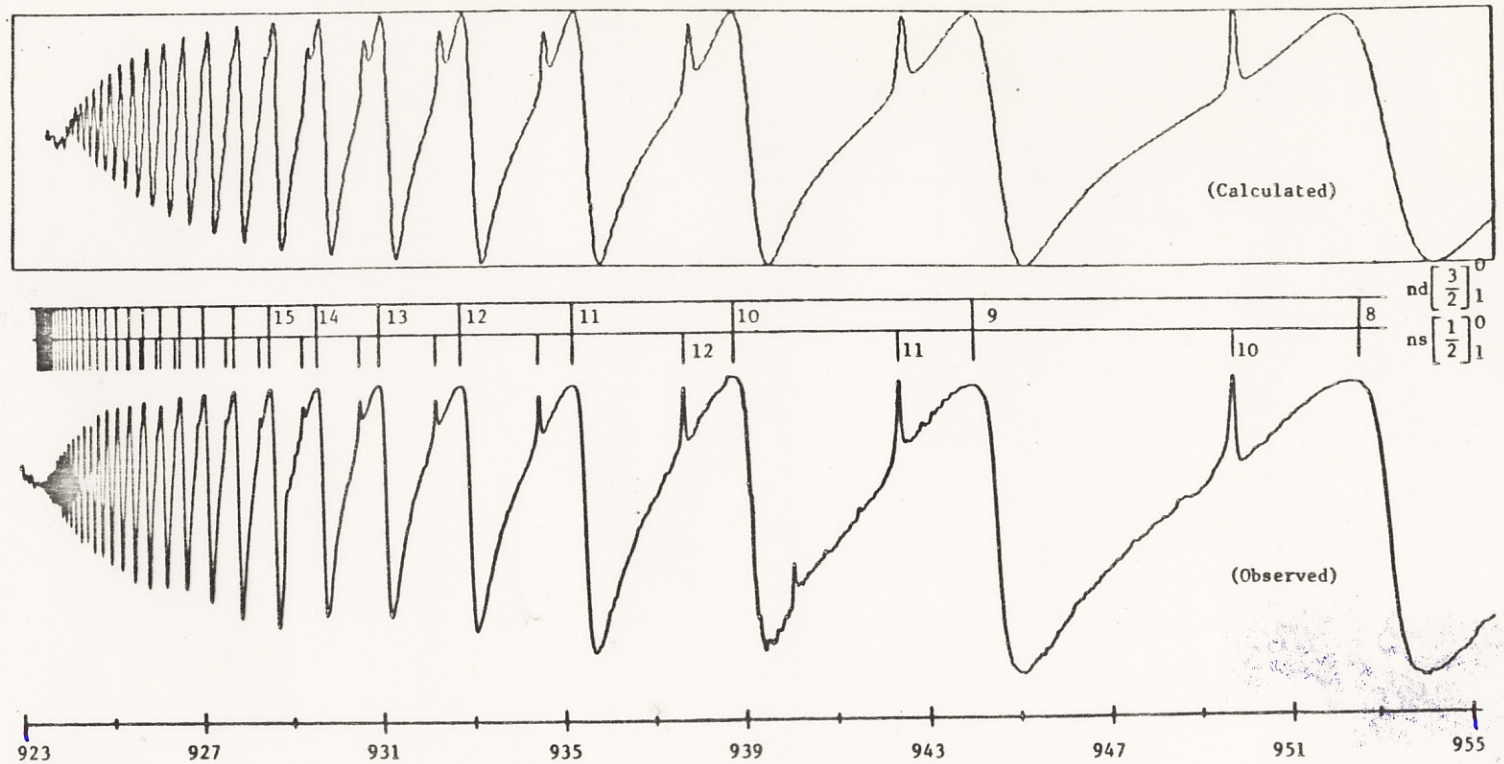

THEORY MQDT

EXPERIMENT

923 A°

955 A°

$$\sigma(E) = A^2(I+E)\,\bar{\sigma}(\nu)$$

$$\bar{\sigma}(\nu) = \frac{\tan^2\pi\nu + 2B\tan\pi\nu + B^2}{\tan^2\pi\nu + 2C\tan\pi\nu + D^2}$$

$$E = E_{lim} - \frac{Z^2}{\nu^2}$$

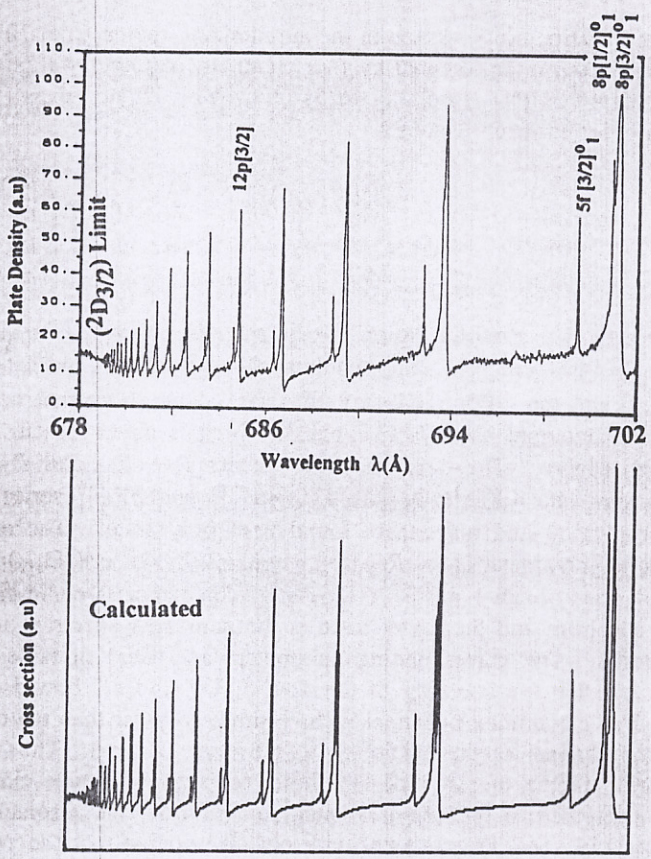

Figure 5. The densitometer trace of the absorption spectrum between 143 000–145 000 cm^{-1}. The Rydberg series are $4d^95s^2(^2D_{5/2})np[\frac{3}{2}]^o_1$, $[\frac{1}{2}]^o_1$ and $nf[\frac{3}{2}]^o_1$. The lower trace shows the calculated spectrum describing the autoionization of the Rydberg series in to the $4d^95s^2(^2D_{5/2})\varepsilon\ell$ continua using a four-channel quantum defect theory model. The corresponding MQDT parameters are given in table 4. An experimental bandwidth of about 3 cm^{-1} was used to average the calculated spectra in order to match the observed spectra.

Table 4. MQDT parameters for the calculation of the photoionization cross section above the $4d^95s^2(^2D_{5/2})$ threshold using the four-channel quantum defect theory model.

Channels	I_i	μ_i	D_i	Reaction matrix R_{ij}	
1 $4d^95s(^2D_{5/2})\varepsilon\ell$			−3.0		
2 $(^2D_{3/2})np[\frac{3}{2}]^o_1$	147 443.7	0.224	2.5	$R_{12} = 0.15$	
3 $(^2D_{3/2})np[\frac{1}{2}]^o_1$	147 443.7	0.199	1.4	$R_{13} = 0.08$	$R_{23} = 0.01$
4 $(^2D_{3/2})nf\,[\frac{3}{2}]^o_1$	147 443.7	0.040	0.8	$R_{14} = 0.05$	$R_{24} = 0.001$

Above the $4d^95s^2(^2D_{5/2})$ limit there are two np and one nf Rydberg series converging to the $4d^95s^2(^2D_{3/2})$ limit (see figures 1 and 5). Although for a proper MQDT analysis one must use as many open channels as there are bound channels but in the observed spectrum there are clear minima in the cross section particularly for the $4d^95s^2(^2D_{3/2})np[\frac{3}{2}]^o_1$ autoionizing resonances. This indicates that the major contribution for autoionization is only from one open channel. Using this assumption, we have used the generalized expression (10) to

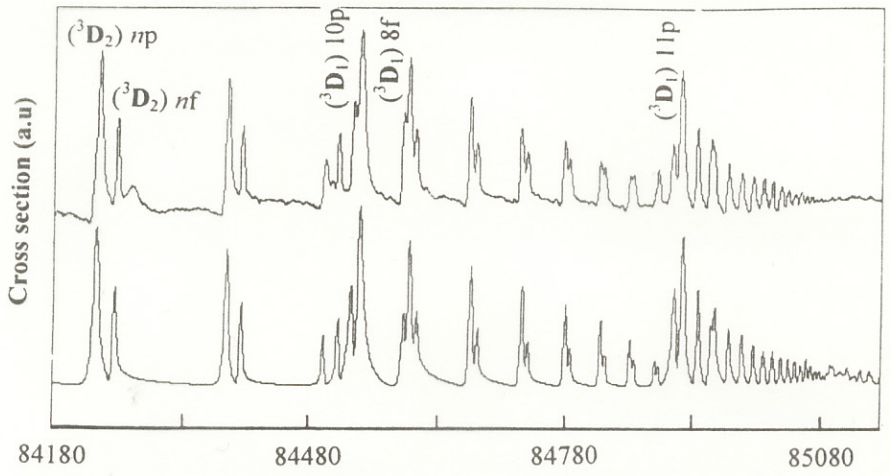

Table 5. MQDT parameters for the calculation of the photoionization cross section between the $3d^94s(^3D_2)$ and $3d^94s(^3D_3)$ thresholds using the six-channel quantum defect theory model.

Channel	I_i	μ_i	D_i	Reaction matrix R_{ij}		
1 $3d^94s(^3D_3)\varepsilon\ell$			−2.5			
2 $3d^94s(^3D_2)np$	84 164	0.170	5.0	$R_{12} = 0.25$		
3 $3d^94s(^3D_2)nf$	84 164	0.054	1.5	$R_{13} = 0.07$	$R_{23} = -0.08$	
4 $3d^94s(^3D_1)np$	85 151	0.170	1.8	$R_{14} = 0.12$	$R_{25} = -0.17$	$R_{35} = 0.04$
5 $3d^94s(^3D_1)np$	85 151	0.157	3.5	$R_{15} = 0.17$	$R_{45} = 0.01$	
6 $3d^94s(^3D_1)nf$	85 151	0.033	1.6	$R_{16} = 0.10$		

Baig et al (1997)

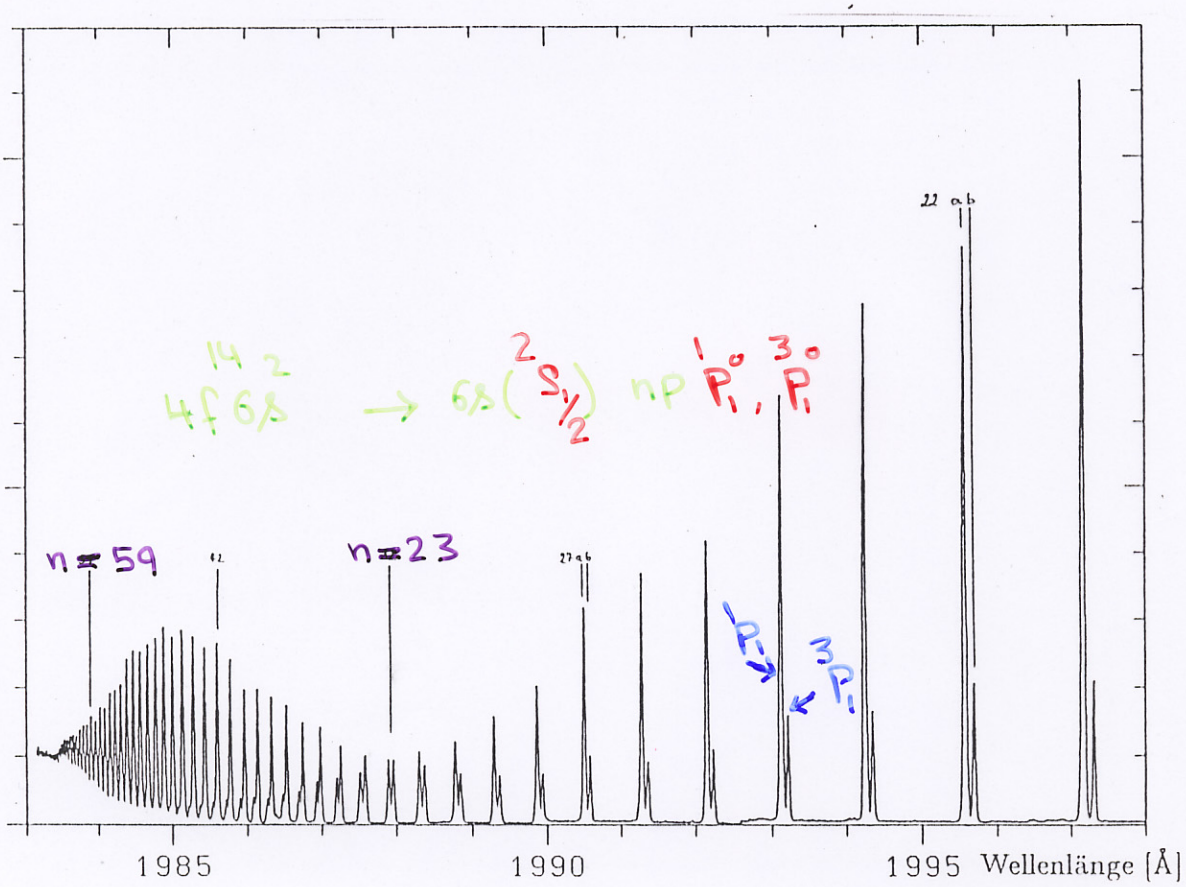
$4f^{14}6s^2 \rightarrow 6s(^2S_{1/2})\,np\ ^1P_1^o, ^3P_1^o$
n = 59
n = 23
$^1P_1$
$^3P_1$
1985
1990
1995 Wellenlänge [Å]

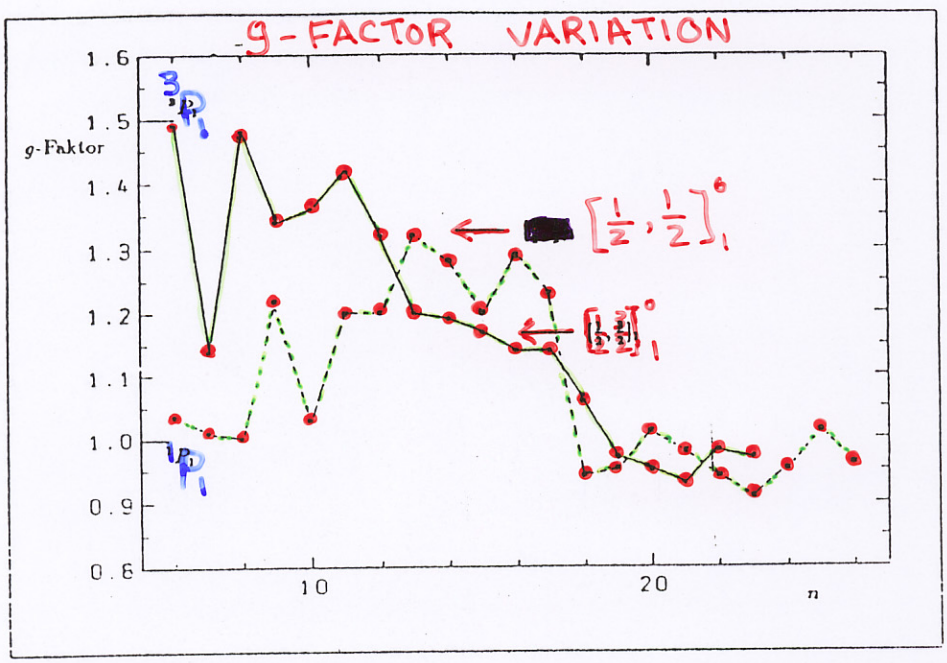
g-FACTOR VARIATION
g-Faktor
1.6
1.5
1.4
1.3
1.2
1.1
1.0
0.9
0.6
10
20
n
$^3P_1$
$^1P_1$
$[\frac{1}{2},\frac{1}{2}]^o_1$
$[\frac{3}{2},\frac{1}{2}]^o_1$

Magneto-optical Rotation

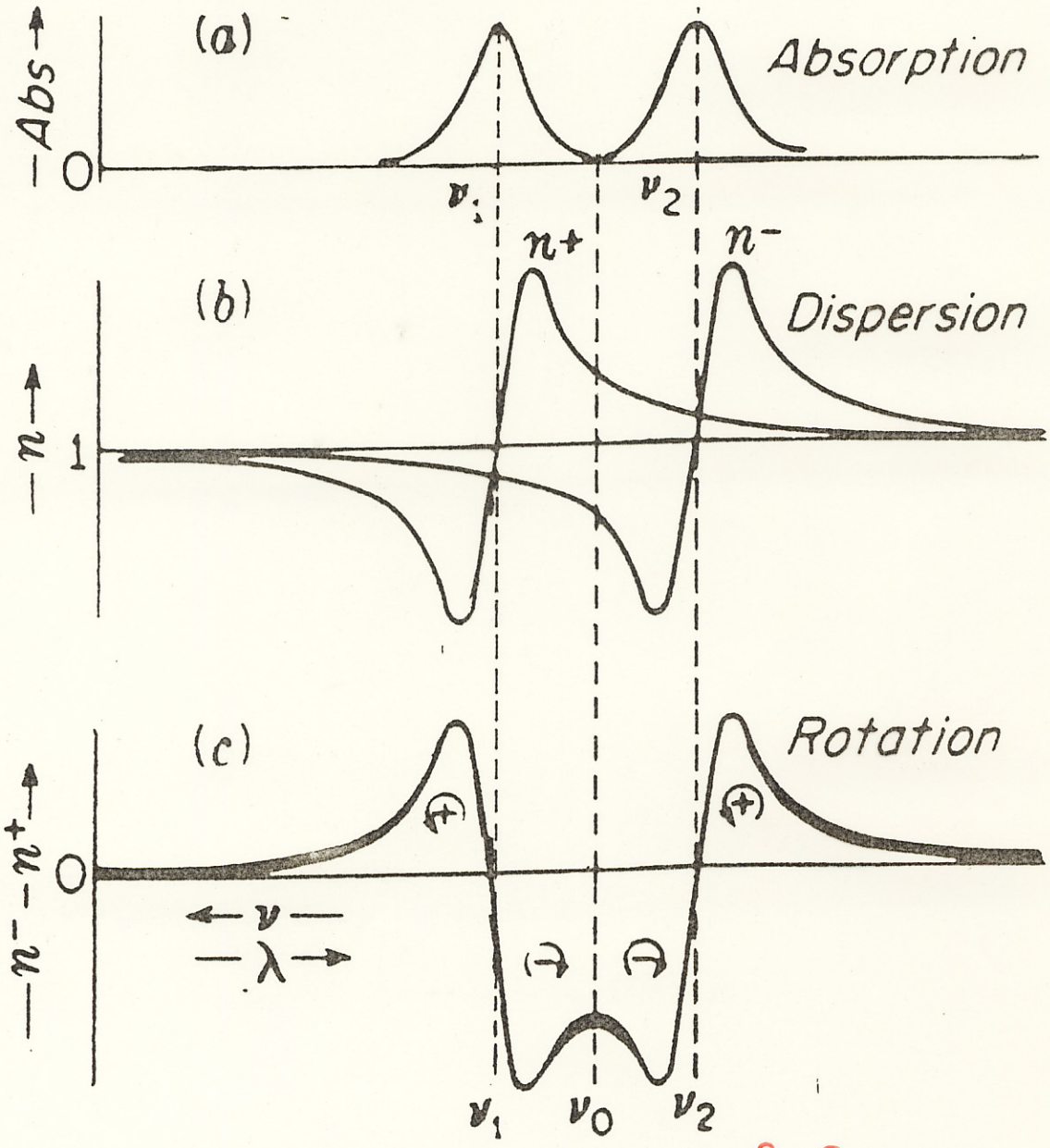

Zeeman splitting: $\Delta\omega_{zee} = \frac{e}{2m} B_g$

Diamagnetic Zeeman effect: $\Delta\omega_{qzee} = \frac{e^2 a_0^2}{m\hbar} \cdot \frac{B^2}{Z^2}(n^4 - n^2)$

Mg: $Z = 12$

B: $B = 5.5$ Tesla

$$\frac{\Delta\omega_{qzee}}{\Delta\omega_{zee}} = 3.5 \times 10^{-7}(n^4 - n^2)$$

$$\simeq 1.5\%$$

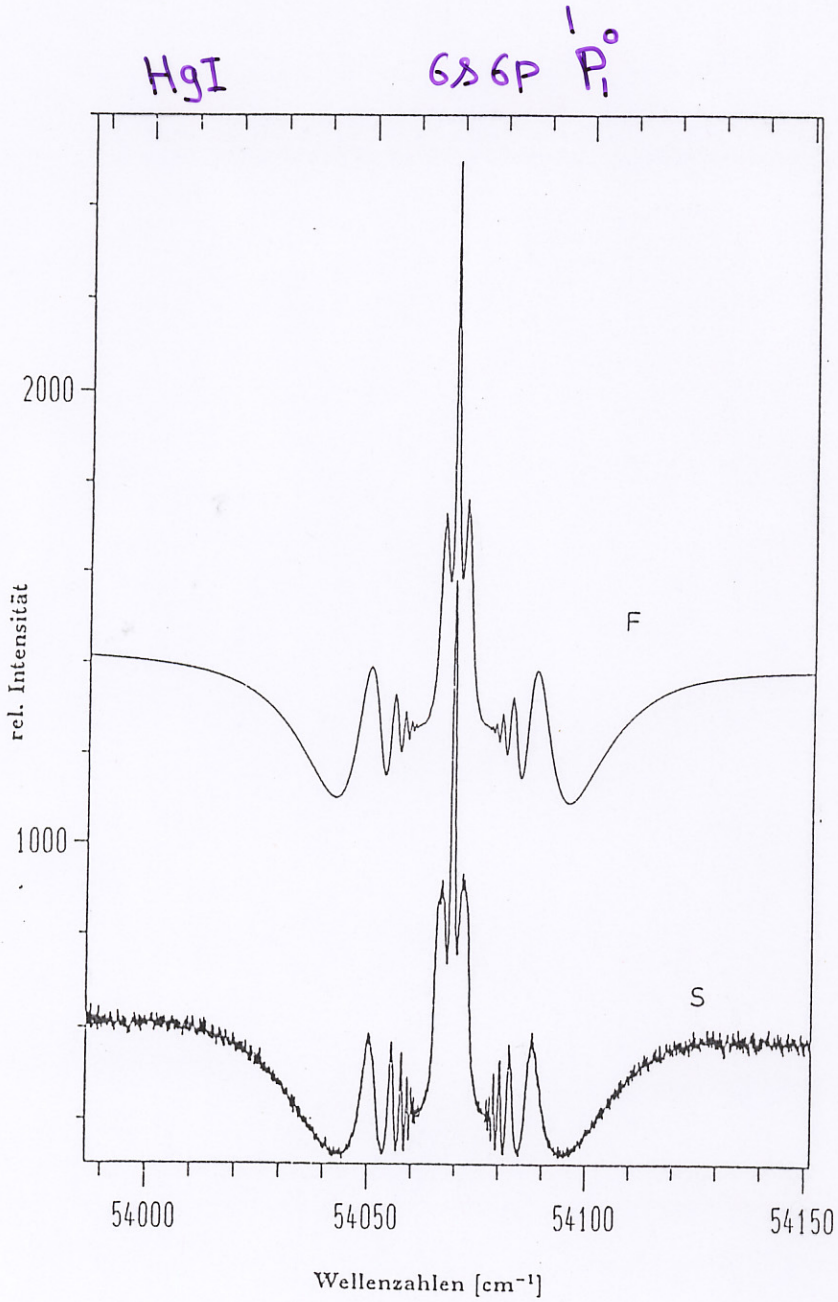

Spektrum (S) und Fit (F) der Hg-1849 Å Linie

Rydberg States of MgI.

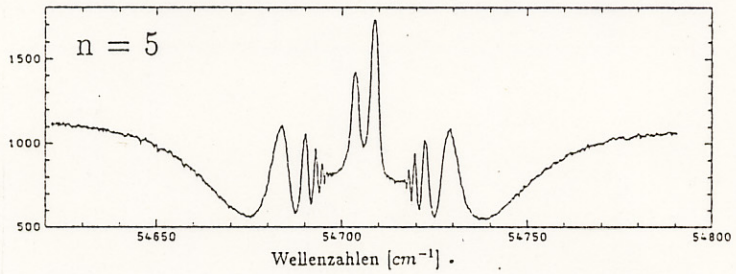

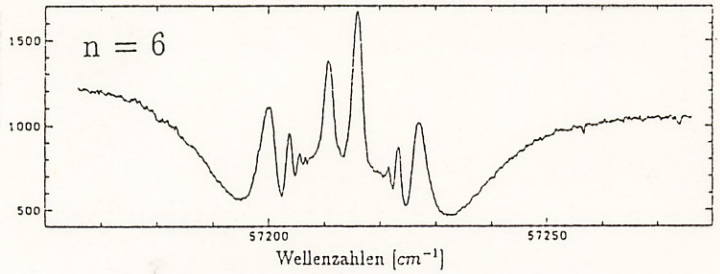

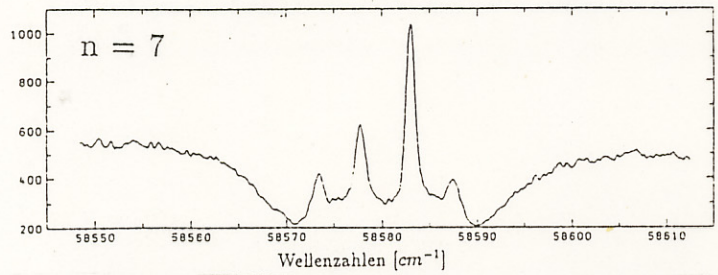

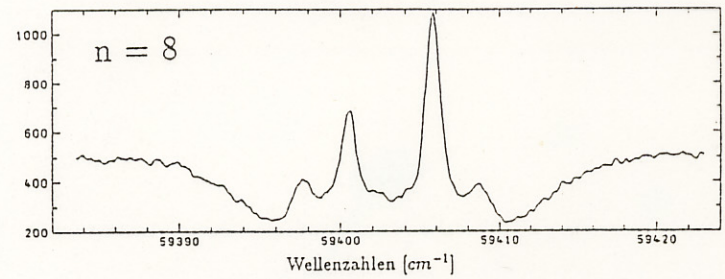

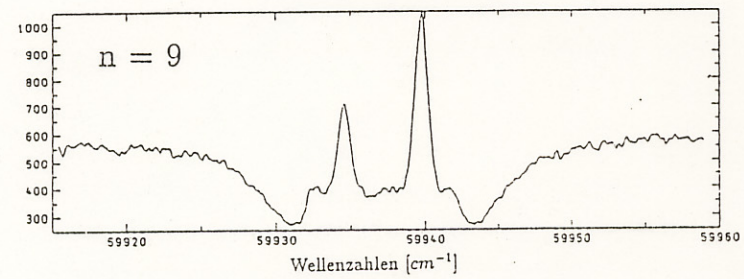

oscillator strengths of Sr I Principal series

n	λ_0 (Å)	n^*	f (present)	f (PS)†	f(PRT)‡
11	2253.954	8.372	0.008 51§	0.008 91 ± 15%	0.008 51 ± 12%
12	2238.350	9.346	0.005 31 ± 0.6%	0.005 25 ± 15%	0.005 13 ± 12%
13	2226.997	10.330	0.003 51 ± 0.7%	0.003 72 ± 15%	0.003 63 ± 12%
14	2218.507	11.319	0.002 58 ± 0.8%	0.002 57 ± 15%	0.002 57 ± 12%
15	2211.999	12.311	0.001 87 ± 1.3%	0.002 09 ± 15%	0.001 86 ± 12%
16	2206.927	13.302	0.001 41 ± 1.5%	0.001 48 ± 15%	0.001 45 ± 15%
17	2202.863	14.302	0.001 10 ± 1.7%	—	0.001 07 ± 15%
18	2199.579	15.301	0.009 24 ± 1.8%	—	0.000 98 ± 15%
19	2196.900	16.294	0.000 696 ± 1.9%	—	0.000 78 ± 15%
20	2194.663	17.292	0.000 555 ± 2.0%	—	0.000 66 ± 15%
21	2192.788	18.290	0.000 447 ± 2.2%	—	0.000 58 ± 15%
22	2191.196	19.293	0.000 378 ± 2.6%	—	0.000 50 ± 20%
23	2189.841	20.288	0.000 309 ± 3.2%	—	0.000 42 ± 20%
24	2188.673	21.286	0.000 268 ± 3.6%	—	0.000 33 ± 20%
25	2187.652	22.288	0.000 218 ± 3.7%	—	0.000 31 ± 20%
26	2186.776	23.273	0.000 179 ± 5.6%	—	0.000 26 ± 20%
27	2186.046	24.281	0.000 149 ± 6.7%	—	—
28	2185.389	25.273	0.000 119 ± 8.3%	—	—

† PS denotes Penkin and Shabanova (1962).
‡ PRT denotes Parkinson, Reeves and Tomkins (1976).
§ All the present values are normalised onto the $n = 11$ f value given by PRT which is regarded as exact when specifying the error bars in the column of present measurements.

Mg I 3s nP $^1P_1$ series

n	n^*	ΔE	Nfl $[10^{14} cm^{-2}]$	ΔNfl[%]	$f \cdot 10^4$	$\frac{f \cdot n^{*3}}{2R} \cdot (eV)$	$f^{-1/3}$
5	3.9694	−0.863	86.401	0.4	556.1	1278.7±5.1	2.62±0.02
6	4.9624	−0.552	28.44	0.8	183.1	822.6±6.6	3.79±0.03
7	5.9584	−0.383	6.385	2	41.10	319.3±9.6	6.24±0.04
8	6.9561	−0.281	3.900	2	25.10	310.6±9.3	7.36±0.05
9	7.9546	−0.215	2.535	3	16.32	302.0±9.0	8.49±0.1
10	8.9533	−0.170	1.505	3	9.69	255.7±7.7	10.1±0.1
11	9.9527	−0.137	1.197	5	7.71	279.5±14.0	10.9±0.2
12	10.9516	−0.113	0.761	5	4.90	236.6±11.8	12.7±0.2
13	11.9513	−0.095	0.682	8	4.39	275.5±22.0	13.2±0.4
14	12.9507	−0.081	0.525	8	3.38	269.9±21.6	14.4±0.4
15	13.9507	−0.070	0.493	10	3.17	316.4±31.6	14.7±0.5
5*	3.9694			5	241.8	556.0±27.8	3.46±0.06
6*	4.9624			5	79.6	357.6±17.9	5.01±0.09

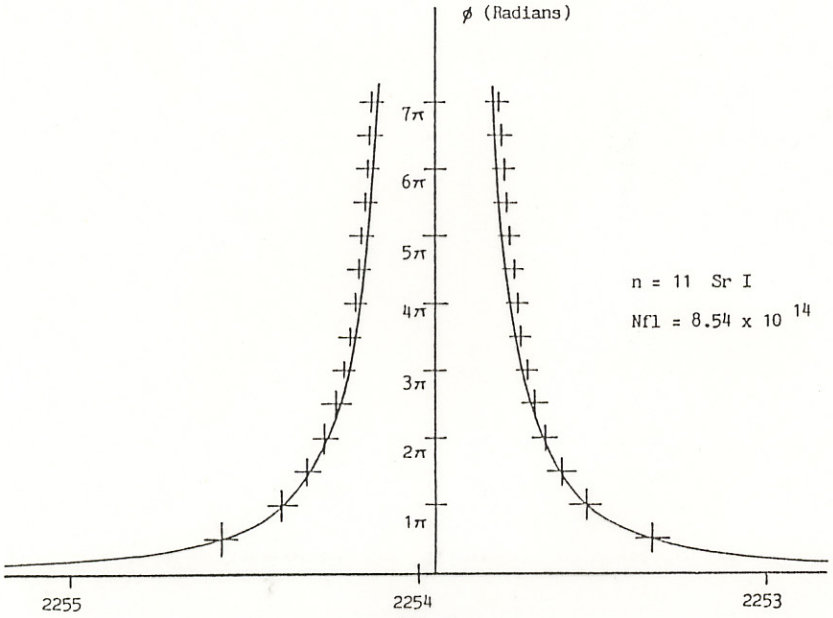

Fig. 4

Magnetic Rotation angle as a function of wavelength (in angstroms) for the far-wings of the pattern in Fig. 3. Notice how the points move off the theoretical curve as one approaches the centre of the pattern, where the sharpest oscillations occur. The accuracy of any analysis based on the far-wing formula is therefore limited.